PROCEEDINGS OF THE ROYAL SOCIETY A

rspa.royalsocietypublishing.org

Research

Article submitted to journal

Subject Areas:
Applied mathematics, Differential equations, Mechanics

Keywords:
non-smooth bifurcation, rotor dynamics, impact with friction, magnetic bearing systems, Hopf-type bifurcation

Author for correspondence:
Karin Mora
e-mail: karin@mora-online.de

Piecewise-smooth Hopf type bifurcations arising from impact/friction contact events in rotating machinery

Karin Mora[1], Chris Budd[1], Paul Glendinning[2], Patrick Keogh[3]

[1]Department of Mathematical Sciences, University of Bath, Claverton Down, Bath BA2 7AY, U.K.,
[2]Centre for Interdisciplinary Computational and Dynamical Analysis (CICADA) and School of Mathematics, University of Manchester, Manchester M13 9PL, U.K.
[3]Department of Mechanical Engineering Sciences, University of Bath, Claverton Down, Bath BA2 7AY, U.K.

We consider novel dynamics arising in the analysis of a nonlinear rotor dynamic system through a full investigation of the discontinuity induced bifurcations corresponding to collisions with the rotor housing (touchdown bearing surface interactions). The simplified Föppl/Jeffcott rotor with clearance and mass unbalance is modelled by a two degree of freedom impact-friction oscillator. Three types of motion have been observed in magnetic bearing systems: no contact, repeated instantaneous contact and continuous contact (rub). We study how these are affected by damping and stiffness present in the system using analytical and numerical non-smooth dynamical systems methods. By studying the impact map, we show that all three types of motion arise at a novel non-smooth Hopf-type bifurcation from a boundary equilibrium bifurcation point for certain parameter values. A local analysis of this bifurcation point allows a complete understanding of this behaviour in a general setting. The analysis identifies criteria for the existence of such smooth and non-smooth bifurcations, which is an essential step towards achieving reliable and robust controllers that can take compensating action.

Royal Society Publishing
Informing the science of the future

1. Introduction

In rotating machines that are levitated by magnetic bearings, non-smooth events involving impact and friction can occur between a rotor and its housing, the stator. These events are undesirable as they may be destructive and hence costly [30]. An understanding of the resulting dynamics, often characterised by new types of non-smooth bifurcations, is a novel contribution and should enable rigorous derivation of possible control strategies. Systems experiencing instantaneous impact and/or friction contact events have been successfully modelled by non-smooth hybrid systems, which model the dynamics of systems with piecewise-smooth flows interrupted by events such as impacts described by maps. These systems experience energy dissipation, which can be modelled by Newton's restitution law and Coulomb's friction law, respectively, [8, 9, 10, 23, 36, 38]. In this paper we adopt this formalism to study a simplified rotating machine, i.e. contact events between a disk (rotor) and a rigid circular boundary (stator) modelled by a 2-degree of freedom impact-friction oscillator. Although other energy dissipation models, such as Poisson's kinetic [20] or Stronge's energetic [28, 33] laws, can be adopted all three are equivalent for this system due to the rotor's properties; we will elaborate the details in §2. The study of such hybrid systems has led to the identification and classification of many discontinuity induced bifurcations such as the non-smooth fold or persistence boundary equilibrium bifurcation (BEB) [8, 9, 10]. These arise when the non-impacting equilibrium evolves to lie on the impact surface under a change of the bifurcation parameter. We will demonstrate that, in a suitable rotating frame, such phenomena occur when considering the rotor motion without contact and in continuous contact (synchronous forward whirl rubbing). However, many more non-smooth related phenomena exist [8, 9] such as creation of limit cycles at BEB and we identify them in this paper.

In general the behaviour of rotating machines such as these can be very complex. Simplified models that do not take rotor damping and/or stiffness into account have been studied in [21, 22]. Li and Païdoussis [21] focus on numerically investigating continuous contact (rub) and repeated impact motion which yields rich dynamics such as chaos as well as non-smooth bifurcation. While Lu *et al*. [21, 22] analytically derive existence conditions of periodically impacting motion. Our intention in this paper is not to give a complete survey of such, but to consider a specific form of motion and the novel Hopf-type bifurcations which lead to this. In particular, Keogh and Cole show [16] that a rotor stator system with damping and friction can exhibit various forms of stable and unstable synchronous single impact limit cycles. We now present a global analysis of the existence of this type of orbit and describe the novel transitions between the aforementioned equilibrium states without impact and *two* coexisting limit cycles with different period at the BEB point. This transition has many of the qualitative features of a smooth Hopf bifurcation in that small amplitude impacting limit cycles of non-zero period are created close to the BEB point. For the sake of classification we shall call it a *non-smooth Fold–Hopf bifurcation*. Our analysis of this transition will be general and applicable to many other related problems.

Similar discontinuity induced Hopf bifurcations, exhibiting a transition of the regular equilibrium to one limit cycle, have been observed in planar piecewise smooth continuous systems [8, 10, 32] with sliding [14] and with biological applications [31]. In vibro-impacting systems of two degrees of freedom non-smooth Hopf bifurcations have been observed and can also be a route to chaos. [23, 38].

In the bifurcation analysis we present in this paper, when studying the effects of bearing damping, we find two coexisting smooth fold bifurcations. We also show the existence of orbits which, at the point of impact, have zero normal velocity and lie tangential to the impact surface, called *grazing* orbits [29].

The remainder of this paper is laid out as follows. In §2, we give a brief introduction to magnetic bearing systems comprising a rotating circular rotor with a disk cross-section impacting with a bearing. We derive the non-dimensionalised equations of the disk in free flight and at impact. In §3 we give examples of the rotor motion in the absence of impact and under impact. In §4 we study boundary equilibrium bifurcations of synchronous non-impacting states. To do this,

the hybrid system approach for modelling systems with instantaneous impact described in [8] is adopted. This procedure reveals standard non-smooth fold and persistence bifurcation for certain parameters. In §5 we apply a Poincaré mapping technique which allows us to determine solutions which are the simplest forms of periodically or quasi-periodically impacting orbit. The resulting global analysis yields interesting and new smooth and non-smooth dynamics described above, including the existence of the non-smooth Hopf-type bifurcations from non impacting equilibria to periodic orbits with impact. In §6 we focus on the local analysis of this Hopf-like bifurcation, looking at a more general class of problems. This analysis allows us to make more a more detailed (local) study of the non-smooth Hopf-type bifurcation and the results can be compared with the calculations in §5. Finally, in §7 we present our conclusions and suggest some open questions.

2. Introduction to magnetic bearing systems and their associated dynamics

Rotating machines are prevalent in engineering applications that require power to be generated or utilised. The power rating is determined by the product of the driving or load torque and the rotational speed. In order to operate effectively, a rotor should spin in a stable manner under the support of bearings. The bearings should also be able to cope with inherent rotor unbalance and any fault conditions that may occur during operation of the machine. A number of bearing types are available to designers of machines, commonly including those based on rolling ball or cylindrical elements, and bushings with oil films. Usually, there is a specified maximum operating speed below which it is safe to run the rotor. If this speed is exceeded for any significant period, the bearing is likely to fail due to high mechanical or thermal stresses. Gas bearings may allow higher speed operation, but they are limited in their load carrying capacity and require a continuous flow of pressurised air. Foil/gas bearings are self-acting and do not require a pressurised source, though below a threshold speed the foil element is in rubbing contact with the rotor and is then prone to wear.

Active magnetic bearings have been under development since the 1970s and have seen a growing number of applications including in turbomolecular and vacuum pumps, compressors, motors, generators, centrifuges, flywheels and beam choppers. An arrangement of electromagnets under feedback control enables a rotor to be levitated. It may then rotate without direct interaction with bearing surfaces or fluids, which has advantages in terms of friction reduction and the elimination of the need for pressurised oil or gas supplies. Higher operating speeds are therefore possible. However, magnetic bearing functionality may be compromised by failure of power supplies, which would lead to rotor delevitation. Also, any external disturbance may cause the load capacity of the bearing, which is limited by magnetic flux saturation, to be exceeded. Magnetic bearings may be configured to transmit low forces at a particular operating speed, through use of a notch filter in the feedback control, but high acceleration input disturbances, e.g. shock conditions, would be problematic. For these reasons, magnetic bearings usually contain secondary touchdown bearings to prevent rotor motion from exceeding damaging limits. The design issues for such systems are given in [24].

Although some studies have been made to investigate the nonlinear rotor dynamics that arise from rotor contact with touchdown bearings, the problem is still not completely understood. The condition for backward whirl, which may involve severe contact forces is understood as the condition in which the rotor is in rolling contact with the touchdown bearing [16]. A number of authors have considered the dynamics of a rotor within a clearance space [1, 3, 5, 6, 7, 11, 12, 15, 17, 18, 26, 27, 37]. With respect to operational magnetic bearing systems, which is in contrast to nonoperational delevitation, it is important to gain a full understanding of all nonlinear dynamic issues so that appropriate control action may be designed to recover contact-free levitation. Without this knowledge it is not possible to ensure that normally levitated control is recoverable.

The mechanical model, illustrated in figure 1, is adopted from [16]. It comprises a spinning rotor with disk cross-section of radius R rotating inside a circular touchdown bearing. At the

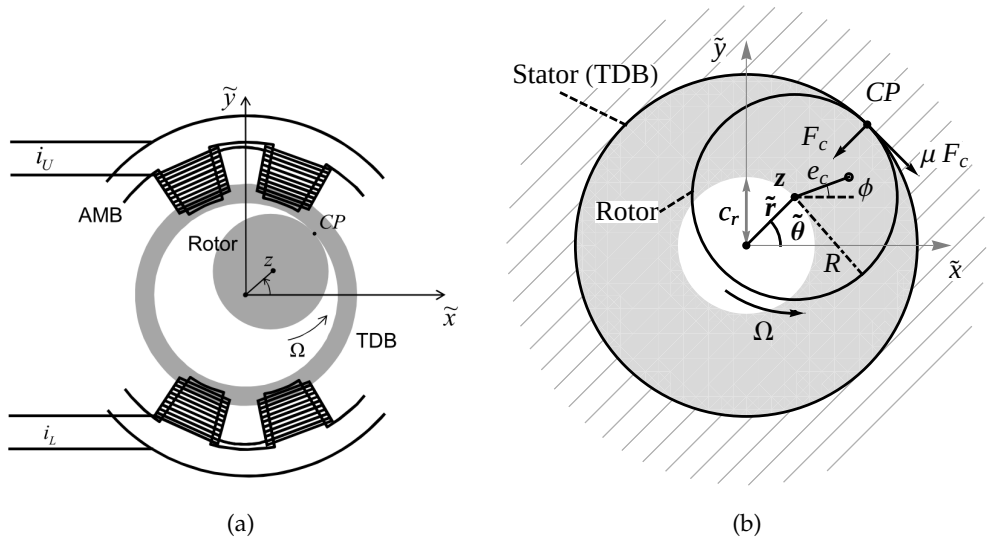

{framework}

Figure 1: Fixed Frame: (a) The active magnetic bearing (AMB) currents, i_U and i_L, are shown in the vertical axis only. With appropriate control, these determine the AMB stiffness and damping characteristic. (b) The rotor-touchdown bearing (TDB) impact at the contact point CP; contact force F_c and frictional force μF_c are acting. The rotor centre is shown in both complex coordinate z and polar coordinates $(\tilde{r}, \tilde{\theta})$. In free flight its motion is constrained to be within the clearance disk (white). The rotor is affected by mass unbalance with eccentricity e_c and phase angle ϕ.

bearing centre lies the origin from which we measure the rotor's position (disk centre) in polar coordinates $(\tilde{r}, \tilde{\theta})$. The rotor comes into contact with the bearing when $\tilde{r} = c_r$. We describe the position of the centre z at time τ using complex coordinates in the form

$$z(\tau) = \tilde{x}(\tau) + i\tilde{y}(\tau) = \tilde{r}(\tau)e^{i\tilde{\theta}(\tau)}.$$

The system under consideration has magnetic bearing supports which are under *proportional-integral-derivative* (PID) control. Then the rotor's motion can be approximated by a linear spring-damper system with stiffness k and damping c, [16]. Further, the rotor, of mass m spinning at constant speed $\Omega > 0$, is affected by mass unbalance. In free flight when the rotor centre, defined by the complex coordinate z, lies within the clearance circle with radius c_r it satisfies a linear constant coefficient complex valued ODE,

$$m\ddot{z}(\tau) + c\dot{z}(\tau) + kz(\tau) = f_u\, e^{i\Omega\tau} \qquad \text{if} \quad |z(\tau)| < c_r \tag{2.1}$$

{eqorig}

where m, c and k are real and positive parameters. The forcing term depends on the angular speed Ω as well as the complex unbalance force f_u, which is given by

$$f_u = m\, e_c\, \Omega^2 e^{i\phi}$$

where e is the unbalance eccentricity (distance between geometric centre and centre of mass) and the unbalance phase ϕ, see figure 1.

It is possible to introduce integral control action in equation (2.1). For real machines the integral (I) gain would be typically set at a level that gives rise to a dynamic mode having a very long time constant. Thus, when the magnetic bearing is activated the integral action ensures that the rotor rises slowly to the bearing centre. Thereafter, it is common to set the integral gain to zero and the established control currents will continue to levitate the rotor at the bearing centre. The remaining proportional (P) and derivative (D) gains will then cause the spring-damper terms to

be effective when the rotor deviates from levitated equilibrium at the magnetic bearing centre. Hence equation (2.1), without integral control action, is representative of a practically levitated and spinning rotor.

We assume that the system experiences an instantaneous collision at time $\tau_{i,-}$ when the rotor centre z comes into contact with the clearance circle, i.e. $|z| = c_r$, and in that case a *reset law* applies. With $\tau_{i,-}$ we denote the impact time as the rotor is approaching the stator and with $\tau_{i,+}$ as the rotor is leaving the stator. Before stating the reset law we will specify our assumptions. First, the stator is assumed to be infinitely stiff and to behave like a fixed impact surface. Second, as the rotational speed Ω is high, the change of Ω during impact is negligible and hence we presume that it remains unchanged during impact. Third, at the point of contact, the relative tangential velocity $v_{rel}(\tau_{i,-})$ between the rotor and frame is given by

$$v_{rel}(\tau_{i,-}) = R\Omega + c_r\dot{\tilde{\theta}}(\tau_{i,-}). \tag{2.2}$$ {vrelcon}

If $\dot{\tilde{\theta}}(\tau_{i,-}) > -R\Omega/c_r$ then the relative tangential velocity does not change sign at impact. We will show that this condition is satisfied for the periodically impacting limit cycles considered in this paper. Hence, it follows that the three coefficient of restitution models, i.e. kinetic, kinematic and energetic, yield the same impact velocity, [28, 33].

Finally, at the impact time $\tau_{i,-}$ the rotor experiences an impulsive normal contact force F_c in the z-direction with an associated impulsive frictional force F_f in the iz-direction. The energy dissipation in the normal contact direction is approximated by Newton's coefficient of restitution d and in the tangential contact direction by Coulomb's coefficient of friction μ. This gives

$$F_f = -\mu\,\mathrm{sgn}(v_{rel}(\tau_{i,-}))F_c = -\mu F_c = -\mu(1+d)m\dot{\tilde{r}}(\tau_{i,-})\delta(\tau - \tau_{i,-}) \tag{2.3}$$

where $\dot{\tilde{r}}(\tau_{i,-})$ is the normal impact velocity and δ is the Dirac delta function.

Under these assumptions the rotor's position is unchanged by the impact:

$$z(\tau_{i,+}) = z(\tau_{i,-}) =: z.$$

In contrast its complex velocity changes instantaneously and satisfies a reset law given by

$$\dot{z}(\tau_{i,+}) = \dot{z}(\tau_{i,-}) - q\frac{\mathrm{Re}(z^*\dot{z}(\tau_{i,-}))z}{|z|^2} = \dot{z}(\tau_{i,-}) - q\dot{\tilde{r}}(\tau_{i,-})\frac{z}{|z|}. \tag{2.4}$$ {resetlaworg}

where $q = (1+d)(1+i\mu)$ and z^* is the complex conjugate of z. Note that although the reset law is nonlinear in the $(\tilde{x}, \tilde{y})$ Cartesian frame with $z = \tilde{x} + i\tilde{y}$, it is linear in the polar coordinates frame $(\tilde{r}, \tilde{\theta})$ and we have

$$\dot{\tilde{r}}(\tau_{i,+}) = -d\dot{\tilde{r}}(\tau_{i,-}) \tag{2.5}$$ {resetlaworg2}

$$\dot{\tilde{\theta}}(\tau_{i,+}) = \dot{\tilde{\theta}}(\tau_{i,-}) - \mu(1+d)\frac{\dot{\tilde{r}}(\tau_{i,-})}{c_r}. \tag{2.6}$$ {resetlaworg3}

There is a range of designs for practical touchdown bearings, including bushing and rolling element types. These are mounted in housings, either directly as push fits or with some compliant backing material to provide some degree of cushioning. A rotor mounted touchdown sleeve may be included as another component. However, a requirement is that the rotor motion must be constrained sufficiently so as to protect the rotor and magnetic bearing. This necessitates that the radial stiffness associated with a touchdown bearing must be significantly greater that associated with a magnetic bearing [30, 34, 35]. Any contact between a rotor and touchdown bearing will generate a finite region of contact, the size of which will depend on material properties and contact force. The contact mechanics will also determine the level of penetration or relative closure of the touchdown bearing and rotor geometric centres under contact. In the limiting case of zero penetration, or infinite contact stiffness, dynamic contact forces become idealised impulsive approximations to the practically finite contact forces. We also remark that considerable uncertainty of contact conditions may arise from angular misalignment between a rotor and touchdown bearing. The impulsive approximation therefore provides an impact model against

which consistent rotor dynamic behaviour may be derived. For this reason, it is adopted in this paper. Predicted rotor motions will generally involve sequences of instantaneous impacts involving impulsive normal and tangential forces. In principle, intervals of persistent contact may be regarded as limiting cases when time intervals between impacts tend to zero [16].

However, for most of the analysis, except for the BEB computation in §4, it is not appropriate to transform the entire system into the latter frame $(\tilde{r}, \tilde{\theta})$ as in this frame the equation of motion (2.1) is nonlinear. It is convenient for further computations to introduce a complex co-rotating frame with coordinate u so that

$$z = ue^{i\Omega\tau}.$$

As the name indicates, this frame rotates synchronously with the rotor at speed Ω. This will be advantageous when examining synchronous impacting limit cycles. It follows that by substituting into the defining equations and cancelling the factor of $e^{i\Omega\tau}$ we have, in free flight,

$$m\ddot{u} + (c + 2im\Omega)\dot{u} + (k - m\Omega^2 + ic\Omega)u = me_c\Omega^2 e^{i\phi}. \tag{2.7}$$ {scale}

A general solution of (2.7) may have an impact at a subsequent time τ_i. In this case the reset law (2.4) in the co-rotating frame becomes

$$\dot{u}(\tau_{i,+}) = \dot{u}(\tau_{i,-}) - (1+d)(1+i\mu)\frac{\mathrm{Re}(u(\tau_i)^*\dot{u}(\tau_{i,-}))u(\tau_i)}{|u(\tau_i)|^2}.$$

where u^* is the complex conjugate of u. We now non-dimensionalise the system both to reduce the number of free parameters and also to show that no natural large or small parameters are present in this system. We introduce a scaled time $t = \Omega\tau$, so

$$\frac{d}{d\tau} = \Omega\frac{d}{dt} \quad \text{and} \quad \frac{d^2}{d\tau^2} = \Omega^2\frac{d^2}{dt^2}.$$

This new term moves through one period in time $t = 2\pi$ if the original time goes through one period of the forcing term, $2\pi/\Omega$. If primes denote differentiation with respect to the scaled time t

$$\ddot{u} = \Omega^2 u'', \quad \dot{u} = \Omega u', \quad \delta(\tau - \tau_{i,-}) = \Omega\delta(t - t_{i,-})$$

then substituting into (2.7) and dividing by $m\Omega^2$ we obtain

$$u'' + \left(\frac{c}{m\Omega} + 2i\right)u' + \left(\frac{k}{m\Omega^2} - 1 + i\frac{c}{m\Omega}\right)u = e_c\, e^{i\phi}. \tag{2.8}$$ {semiscale}

Setting the parameters

$$\gamma = \frac{c}{m\Omega}, \quad \omega^2 = \frac{k}{m\Omega^2} \quad \text{and the variable} \quad u = c_r U$$

then (2.8) in scaled co-rotating complex coordinate $U := re^{i\theta}$ becomes

$$\ddot{U} + (\gamma + 2i)\,\dot{U} + (\omega^2 - 1 + i\gamma)\,U = \rho\, e^{i\phi} \quad \text{in} \quad |U| \le 1 \tag{2.9}$$ {eqrescale}

where $\rho = e_c/c_r$. The corresponding inertial complex coordinate $Z := re^{\Theta}$ with $\Theta := \theta + t$. Consequently, the reset law is

$$U(t_+) = U(t_-) \tag{2.10}$$

$$\dot{U}(t_+) - \dot{U}(t_-) = -q\,\dot{r}(t_-)U(t_-) \tag{2.11}$$ {implaw}

where $\dot{r}(t_-)$ is the normal velocity in polar coordinates and $q = (1+d)(1+i\mu)$. The choices of parameters (in consistent units) corresponding to the experimental application in [16] are

$$m = 50\ \text{kg}, \quad c = 1400\ \text{N s/m}, \quad k = 9.8\times10^5\ \text{N/m}, \quad e_c = 0.3\times10^{-3}\ \text{m}, \quad c_r = 0.7\times10^{-3}\text{m},$$
$$R = 0.4\times10^{-1}\ \text{m}, \quad \phi = 0.21\ \text{rad}, \quad \Omega = 184.2\ \text{rad/s}, \quad \mu = 0.15, \quad d = 0.95$$

and the revised parameters, valid in the unit disk after rescaling are

$$\gamma \approx 0.152, \quad \omega \approx 0.76, \quad \rho = 3/7 \approx 0.428, \quad \mu = 0.15, \quad d = 0.95$$

i.e. all the parameters are now order one and there are no privileged small or large parameters. In this paper the bearing damping coefficient $\gamma > 0$ will act as the bifurcation parameter and the remaining parameters will take the values given above.

3. Basic solution types of synchronous rotor dynamics

{basicsolsec}

In this section we introduce the basic simplest solution types in the co-rotating frame, and in particular study solutions which are either not in contact, or are in continuous contact, or which have instantaneous impacts. To do this we firstly, we rewrite the scaled equations of motion (2.9) as a first order complex system. This will be helpful in the global and local analysis of a periodically impacting orbit in later sections. Let the complex vector $\boldsymbol{w} = (U, \dot{U})$, then

$$\dot{\boldsymbol{w}}(t) = A\boldsymbol{w}(t) + \boldsymbol{b} \tag{3.1}$$

{veceqn}

where the matrix A and the vector $\boldsymbol{b}$ are constant and are defined by

$$A = \begin{pmatrix} 0 & 1 \\ 1-\omega^2 - i\gamma & -\gamma - 2i \end{pmatrix} \quad \text{and} \quad \boldsymbol{b} = \begin{pmatrix} 0 \\ \rho e^{i\phi} \end{pmatrix}. \tag{3.2}$$

{matAvb}

As this equation is linear and the vector $\boldsymbol{b}$ is a constant the general solution with initial conditions $\boldsymbol{w}(t_{0,+})$ can be written as

$$\begin{aligned} \boldsymbol{w}(t) &= \exp(A(t-t_0))\left(\boldsymbol{w}_{0,+} + A^{-1}\boldsymbol{b}\right) - A^{-1}\boldsymbol{b} \qquad \text{if} \quad |U| \leq 1 \\ \boldsymbol{w}_{0,+} &= \boldsymbol{w}_{0,-} - \begin{pmatrix} 0 \\ q\dot{r}_{0,-}U_0 \end{pmatrix} \qquad \text{if} \quad |U| = 1 \end{aligned} \tag{3.3}$$

{trajG}

where $q = (1+d)(1+i\mu)$ and we simplify the notation $\boldsymbol{w}(t_{0,+}) \equiv \boldsymbol{w}_{0,+}$. The eigenvalues $\lambda_\pm$ of the matrix A are given by

$$\lambda_\pm = \frac{-\gamma + i\left(-2 \pm \sqrt{4\omega^2 - \gamma^2}\right)}{2} \tag{3.4}$$

{evalsA}

with real part $\mathrm{Re}(\lambda) = -\gamma/2 < 0$ as we assume (given the experimentally defined values) that $0 < \gamma < 2\omega$. This implies that in the absence of impact there is an asymptotically stable equilibrium solution given by

$$\boldsymbol{w} = -A^{-1}\boldsymbol{b}. \tag{3.5}$$

{eq:equilibrium}

Depending on the parameters this equilibrium can lie either

(i) inside (equilibrium is physically realistic, we denote this steady state *admissible*)
(ii) on: (continuous contact) or
(iii) outside: (equilibrium is physically unrealistic, we denote this steady state *virtual*)

the clearance circle. By extension, this nomenclature is implemented for other orbits. In the first case this motion is called non-contacting whirl, figure 2a. The second case describes the critical transition point between physically realistic (case 1) and physically unrealistic orbits (case 3). Due to rotor faults, such as rotor unbalance or mass loss, more complicated rotor trajectories are possible, such as those involving continuous (zero normal velocity and non-negative normal acceleration) or instantaneous rotor-stator contact. When the rotor and stator are in continuous contact, sliding [16] or pure rolling (if relative tangential velocity $v_{rel}(t) = 0$, e.g. [16]), are possible. In the case of sliding, forward whirl rubbing is observed if $\dot{\theta}(t) > 1$ (in the co-rotating frame), and backward whirl rubbing if $\dot{\theta}(t) < 1$ (in the co-rotating frame). In this paper we consider only one particular type of continuous contact called synchronous forward whirl rubbing, i.e. in the co-rotating frame the rotor sticks to the stator (tangential velocity $\dot{\theta}(t) = 0$), e.g. [16]. In particular, we will only study the equilibria of this kind of motion and show that standard non-smooth bifurcations with the non-impacting equilibrium occurs in §4. Other continuous

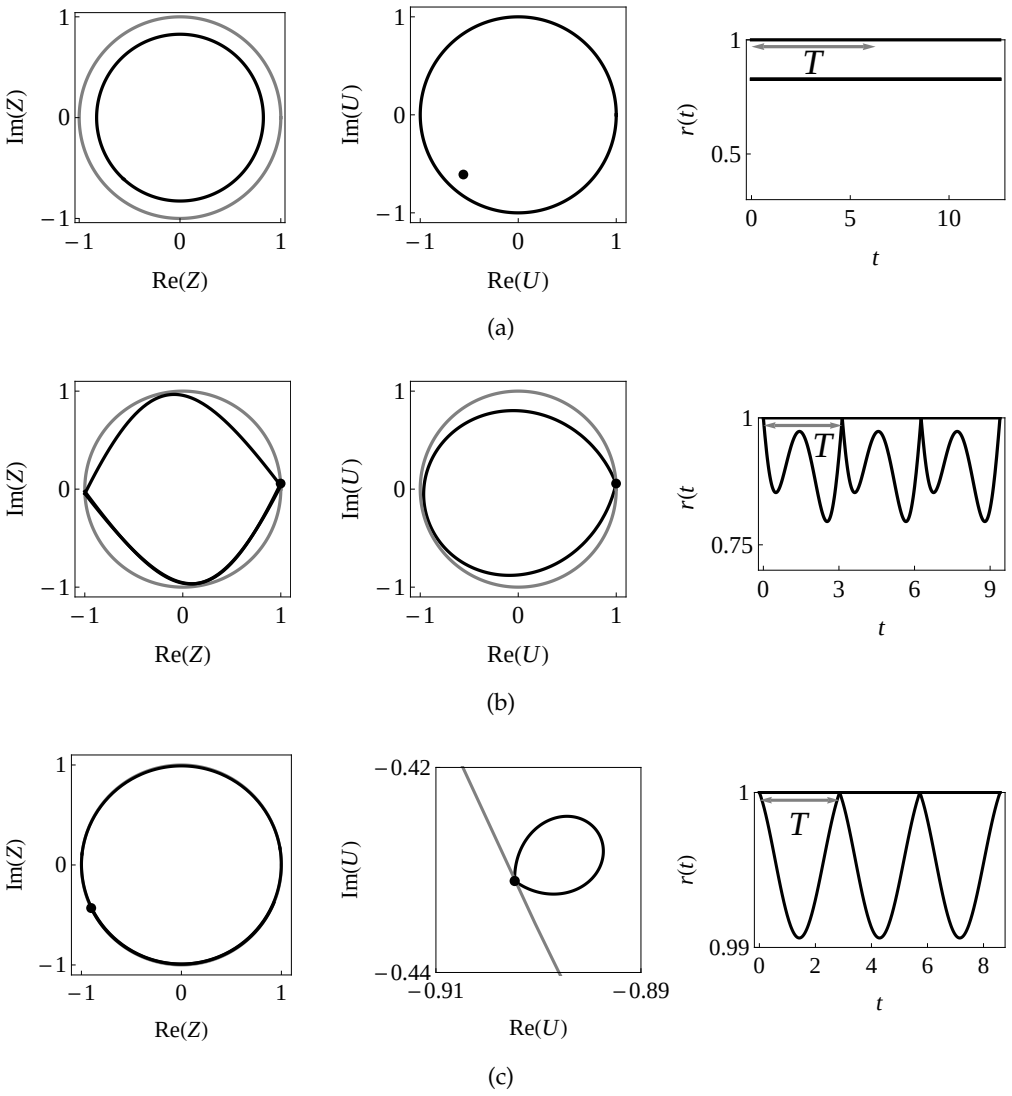

{exorba}

{exorbb}

{exorbc}

Figure 2: Orbits (black) with period T in the inertial and the rotating frame as well as amplitude $r(t)$ against time t. The clearance circle (grey) has radius 1. 2a Regular equilibrium without impact ($\gamma = 0.3$). 2b Limit cycle $B_{1,d}$ near grazing ($\gamma = 0.065$). 2c Limit cycle $B_{1,a}$ near non-smooth Fold–Hopf Bifurcation, ($\gamma = 0.1$).

{exorb}

contact motions are not studied in this paper as the reset law is not sufficient to describe such behaviour and how it arises.

When the rotor and stator experience an instantaneous contact it can lead to orbits that impact periodically or quasi-periodically and synchronously in the co-rotating frame, figures 2b, 2c. We call these *period* 1 *synchronous impacting limit cycles* as the orbit experiences one impact per period. The limit cycles with small amplitude (figure 2c) are created in a non-smooth Hopf-type bifurcation, see §5. Whereas limit cycles with large amplitude (figure 2b) can lead to grazing events [29], i.e. the trajectory interacts tangentially with the impact surface. A systematic way of analysing such motions with instantaneous impact, is to consider them as orbits of hybrid piecewise-smooth dynamical systems, in which smooth flows between impact are combined with

maps describing the impact. Such an approach is very suitable for finding both the existence and the stability of periodic orbits [9] and we will adopt it here.

In addition to periodic [22, 25] or quasi-periodic orbits [21, 25] it has been shown that in similar models the rotor-stator motion can be chaotic [21, 25]. Other types of motion can include an accumulation of infinite number of impacts in finite time [13, 21, 25], often called *chattering*. Chattering can lead to sticking [4] and sliding motion [9] and hence can be used to predict the onset of continuous contact motion without actually computing continuous contact trajectories. Li and Païdoussis [21] have done this to identify for what values of coefficient of friction, μ, and eccentricity, e_c, continuous contact motion occurs. Similarly, the occurrence of chattering sequences and the possibly resulting continuous contact also depends on damping, c, and spring stiffness, k, parameters [25]. Such, particle motion can best be systematically described by set valued functions instead of hybrid systems. These types of models, called *differential inclusion* [19] are particularly well suited to analyse problems involving only friction, e.g. sliding and sticking motion of rotating particles. Such a model, a forced rotating pendulum in continuous contact with a circular boundary, shows similar features to ours in that various orbits collapse onto the equilibrium set in finite time [2]. Whilst it is certainly possible that such chattering and sticking motions may arise in a magnetic bearing system, in this paper we will restrict or analysis to that of the simpler types of periodic motion described above.

4. Boundary equilibrium solutions and their bifurcations

{BEBsec}

Boundary equilibria are steady states of the form (3.5) that lie on the impact surface, so that $|U| = c_r$. They are important in the bifurcation analysis of non-smooth systems as other equilibria or limit cycles can bifurcate from them. In this section we focus on the system's equilibria of both motion in free flight and in continuous contact (only sticking), called *regular* and *pseudo* equilibria respectively, in the co-rotating frame. The standard theory developed in [8, 9, 10] will be applied to study their existence and stability and categorise the bifurcation scenarios. Depending on the system's parameters we will observe either *persistence* or a *non-smooth fold*. In the first case a regular equilibrium becomes a pseudo equilibrium as the bifurcation parameter γ is varied. In the second case these two are created in a fold like bifurcation and coexist.

The analysis using the methods mentioned above is much simpler when the reset law is linear; this is the case when the system (2.9) is formulated in polar coordinates. Let the state vector of the rotor centre in polar coordinates $\boldsymbol{x} \in \mathbb{R}^4$ be given by

$$\boldsymbol{x} = (x_1, x_2, x_3, x_4) := (r, \theta, \dot{r}, \dot{\theta}).$$

In contrast, its motion in free flight (2.9) is now given by the nonlinear system

$$\dot{\boldsymbol{x}} = F(\boldsymbol{x}), \quad H(\boldsymbol{x}) := 1 - x_1 > 0 \tag{4.1}$$

where

$$F(\boldsymbol{x}) = \begin{pmatrix} x_3 \\ x_4 \\ x_1\left((1+x_4)^2 - \omega^2\right) - \gamma x_3 + \rho\cos(\phi - x_2) \\ \left(-(1+x_4)(\gamma x_1 + 2x_3) + \rho\sin(\phi - x_2)\right)/x_1 \end{pmatrix}.$$

An impact is observed when the state vector $\boldsymbol{x}$ lies on the impact surface Σ defined by

$$\Sigma = \{\boldsymbol{x} : H(\boldsymbol{x}) := 1 - x_1 = 0\} \tag{4.2}$$

{impsurf}

in which case the reset law R applies. The state after impact $\boldsymbol{x}^+$ is given by

$$\boldsymbol{x}^+ = R(\boldsymbol{x}^-) = \boldsymbol{x}^- + W(\boldsymbol{x}^-)v(\boldsymbol{x}^-)$$

where the vector $W = (0, 0, 1+d, \mu(1+d))^T$. Let $v(\boldsymbol{x})$ be the velocity of the vector field F relative to H, denoted by

$$v(\boldsymbol{x}) := H_{\boldsymbol{x}} F(\boldsymbol{x}) = -x_3 \tag{4.3}$$

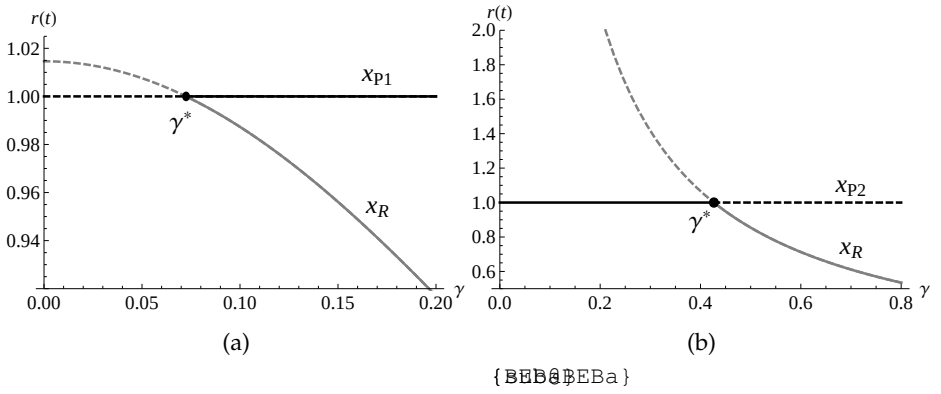

Figure 3: Bifurcation scenario of regular (grey) and pseudo (black) equilibria. (a) Virtual (dashed) regular $\boldsymbol{x}_R$ and pseudo $\boldsymbol{x}_{P1}$ equilibria clash in a non-smooth fold bifurcation at $\gamma^* \approx 0.072$ and become admissible (solid). (b) The admissible pseudo equilibrium x_{P2} and virtual regular equilibrium $\boldsymbol{x}_R$ become virtual and admissible, respectively, in a persistence bifurcation at $\gamma^* \approx 0.428$.

and let $a(\boldsymbol{x})$ be the respective acceleration given by

$$a(\boldsymbol{x}) := (H_{\boldsymbol{x}}F)_{\boldsymbol{x}}F(\boldsymbol{x}) = -\dot{x}_3. \tag{4.4}$$

In the special case when the normal velocity x_3 is zero, the reset law R is the identity mapping.

Next, we will describe the motion in continuous contact. The rotor centre undergoes sticking motion (in the co-rotating frame) when it comes into contact with the boundary, i.e. $H = 0$, and remains there, i.e. when the velocity $v(\boldsymbol{x}) = 0$ and the acceleration $a(\boldsymbol{x}) < 0$, called sticking conditions. The motion, which is degenerate, is maintained along the vector field F_s, as defined by

$$F_s(\boldsymbol{x}) := F(\boldsymbol{x}) - \eta(\boldsymbol{x})W(\boldsymbol{x}) = \begin{pmatrix} x_3 \\ x_4 \\ 0 \\ \big(-(1+x_4)(\gamma x_1 + 2x_3) + \rho\sin(\phi - x_2) - \mu(1+d)\,\eta\,(\boldsymbol{x})\big)/x_1 \end{pmatrix}$$

where η, chosen such that the sticking conditions are satisfied, is given by

$$\eta(\boldsymbol{x}) := \frac{a(\boldsymbol{x})}{(H_{\boldsymbol{x}}F)_{\boldsymbol{x}}W(\boldsymbol{x})} = \frac{-1}{1+d}\left(x_1(\omega^2 - (1+x_4)^2) - \gamma x_3 - \rho\cos(\phi - x_2)\right).$$

As η depends on the acceleration $a(\boldsymbol{x})$ its sign determines when the sticking vector field is physically realistic, i.e. $\eta(\boldsymbol{x}) > 0$. In an impacting system with these two motions the following equilibria can be observed; the admissible equilibrium of the steady state:

E1 of free flight motion called *regular equilibrium* $\boldsymbol{x}_R$ if $F(\boldsymbol{x}_R) = 0$ and $H(\boldsymbol{x}_R) > 0$ hold,
E2 of sticking motion called *pseudo equilibrium* $\boldsymbol{x}_P$ if $F_s(\boldsymbol{x}_P) = 0$, $H(\boldsymbol{x}_P) = 0$ and $\eta(\boldsymbol{x}_P) > 0$ hold.

The regular equilibrium is called virtual if it lies outside of the stator boundary, i.e. $H(\boldsymbol{x}_R) < 0$. The pseudo equilibrium is called virtual if the acceleration points away from the stator, i.e. $\eta(\boldsymbol{x}_P) < 0$.

We are interested in when these two equilibria bifurcate. In an impacting system this happens when the regular equilibrium lies on the impacting surface. This is called *boundary equilibrium point* at $\boldsymbol{x} = \boldsymbol{x}_B$ with $\gamma = \gamma^*$ if $F(\boldsymbol{x}_B, \gamma^*) = 0$ and $H(\boldsymbol{x}_B, \gamma^*) = 0$ hold.

We claim that our system has one regular equilibrium (non-impacting whirl) given by

$$\boldsymbol{x}_R = \left(\frac{\rho}{\sqrt{\gamma^2 + (-1+\omega^2)^2}}, \phi - \pi + \arctan\left(\frac{\gamma}{1-\omega^2}\right), 0, 0 \right),$$

but two pseudo equilibria (synchronous forward whirl rubbing)

$$\boldsymbol{x}_{P1,P2} = \left(1, \phi - \pi \mp \arccos\left(\frac{\gamma + \mu(1-\omega^2)}{\rho\sqrt{1+\mu^2}} \right) + \arctan\left(\frac{1}{\mu}\right), 0, 0 \right),$$

with the sticking vector field admissibility condition given by

$$\eta_{1,2} = \frac{1 - \omega^2 - \gamma\mu \mp \sqrt{\rho^2(1+\mu^2) - (\gamma + \mu(1-\omega^2))^2}}{(1+d)(1+\mu^2)}.$$

Before we state the bifurcation scenario at the boundary equilibrium point

$$\boldsymbol{x}_B = \left(1, \phi - \pi + \arctan\left(\frac{\sqrt{\rho^2 - (-1+\omega^2)^2}}{1-\omega^2} \right), 0, 0 \right) \quad \text{with} \quad \gamma^* = \sqrt{\rho^2 - (-1+\omega^2)^2}$$

of this system we briefly explain the methods developed in [8, 9, 10].

Linearising about the boundary equilibrium point $\boldsymbol{x}_B$ with γ^* yields the conditions which determine how the regular and pseudo equilibrium bifurcate at that point. Assuming that the following conditions hold

(C1) $\det(F_{\boldsymbol{x}}^{-1}(\boldsymbol{x}_B, \gamma^*)) \neq 0$

(C2) $H_\gamma(\boldsymbol{x}_B, \gamma^*) - H_{\boldsymbol{x}}(\boldsymbol{x}_B, \gamma^*)\, F_{\boldsymbol{x}}^{-1}(\boldsymbol{x}_B, \gamma^*)\, F_\gamma^{-1}(\boldsymbol{x}_B, \gamma^*) \neq 0$

(C3) $-H_\gamma(\boldsymbol{x}_B, \gamma^*)\, F_{\boldsymbol{x}}^{-1}(\boldsymbol{x}_B, \gamma^*)\, W(\boldsymbol{x}_B, \gamma^*) \neq 0$

two bifurcation scenarios can occur. *Persistence* describes the situation when the admissible pseudo equilibrium becomes an admissible regular equilibrium, or vice versa. This is the case when the following inequality holds

(C4) $-H_\gamma(\boldsymbol{x}_B, \gamma^*)\, F_{\boldsymbol{x}}^{-1}(\boldsymbol{x}_B, \gamma^*)\, W(\boldsymbol{x}_B, \gamma^*) < 0.$

A *non-smooth fold* bifurcation takes place when the admissible regular and pseudo equilibrium are created in a fold like bifurcation and coexist as the bifurcation parameter γ is changed in one direction but not the other; they cease to exist in one direction as they are not conceivable in a physical sense. Assuming the same conditions as for the previous bifurcation scenario the opposite inequality must hold:

(C5) $-H_\gamma(\boldsymbol{x}_B, \gamma^*)\, F_{\boldsymbol{x}}^{-1}(\boldsymbol{x}_B, \gamma^*)\, W(\boldsymbol{x}_B, \gamma^*) > 0.$

Now, we can state our results and explain all the details of this system's bifurcation scenario. For an example of these scenarios with particular parameters see figure 3. Combining these results we have established the following.

{propBEB}

Proposition 4.1. *Assume that the scaled spring constant $\omega \in (0,1)$, scaled unbalance radius $\rho \in (0,1)$, coefficient of restitution $d \in (0,1)$ and friction constant $\mu \in (0,1)$. Then at the boundary equilibrium point $\boldsymbol{x}_B$ with γ^* conditions (C1-3) are satisfied and we observe:*

a non-smooth fold *bifurcation of the regular equilibrium $\boldsymbol{x}_R$ and the pseudo equilibrium $\boldsymbol{x}_{P1}$ if*

$$\sqrt{1-\rho} < \omega < \sqrt{1 - \frac{\mu\rho}{\sqrt{1+\mu^2}}}. \tag{4.5}$$ {omcond}

The two equilibria, $\boldsymbol{x}_R$ and $\boldsymbol{x}_{P1}$, coexist for $\gamma \in (\gamma^*, 1)$ while the second pseudo equilibrium $\boldsymbol{x}_{P2}$ exists for all $\gamma \in (0,1)$.

a persistence *bifurcation of the regular equilibrium* $\boldsymbol{x}_R$ *and the pseudo equilibrium* $\boldsymbol{x}_{P2}$ *if*

$$\sqrt{1-\frac{\mu\rho}{\sqrt{1+\mu^2}}}<\omega<1.$$

Then, no equilibrium coexists as the pseudo equilibrium $\boldsymbol{x}_{P1}$ *is virtual and* $\boldsymbol{x}_{P2}$ *exists for* $\gamma\in(0,\gamma^*)$ *while* $\boldsymbol{x}_R$ *exists for* $\gamma\in(\gamma^*,1)$.

Note that $\omega>\sqrt{1-\rho}$ as otherwise the scaled damping parameter γ^* at the boundary equilibrium point is complex. Also, without damping, i.e. if $\gamma=0$ the rotor in free motion is purely oscillatory.

We complete this section with the stability analysis of the three equilibria $\boldsymbol{x}_R$, $\boldsymbol{x}_{P1}$ and $\boldsymbol{x}_{P2}$ as well as the boundary equilibrium point $\boldsymbol{x}_B$ with γ^*. The Jacobian matrix at the regular equilibrium is given by

$$F_{\boldsymbol{x}}(\boldsymbol{x}_R)=\begin{pmatrix}0 & 0 & 1 & 0\\ 0 & 0 & 0 & 1\\ 1-\omega^2 & \gamma\rho/\ell_1 & -\gamma & 2\rho/\ell_1\\ -\gamma\ell_1/\rho & 1-\omega^2 & -2\ell_1/\rho & -\gamma.\end{pmatrix}$$

where $\ell_1=\sqrt{\gamma^2+(\omega^2-1)^2}$. This matrix has four distinct eigenvalues Λ given by

$$\Lambda_R=\frac{1}{2}\left(-\gamma\pm 2i\pm i\sqrt{4\omega^2-\gamma^2}\right)$$

We assume the scaled damping constant γ is positive and hence it follows that the regular equilibrium $\boldsymbol{x}_R$ is stable as $\mathrm{Re}(\Lambda_R)<0$ for all $\gamma>0$.

In order to determine the stability of the pseudo equilibria within the sticking set we study the Jacobian of the sticking vector field at the pseudo equilibria, given by

$$F_{s,\boldsymbol{x}}(\boldsymbol{x}_{P1,P2})=\begin{pmatrix}0 & 0 & 1 & 0\\ 0 & 0 & 0 & 1\\ 0 & 0 & 0 & 0\\ \frac{\gamma+\mu^3(-1+\omega^2)\pm\mu\ell_2}{1+\mu^2} & \frac{2\gamma\mu+2\mu^2(1-\omega^2)\pm(1-\mu^2)\ell_2}{1+\mu^2} & -2+\gamma\mu & -\gamma-2\mu\end{pmatrix}$$

where $\ell_2=\sqrt{-\left(\gamma+\mu(1-\omega^2)\right)^2+\rho^2(1+\mu^2)^2}$. Two eigenvalues of this matrix are zero as the sticking vector field is degenerate due to the conditions which maintain the motion on the impact surface. But the other two eigenvalues do determine the stability of each pseudo equilibria $\boldsymbol{x}_{P1}$ and $\boldsymbol{x}_{P2}$ which are given by

$$\Lambda_{P1}=\frac{1}{2}\left(\gamma-2\mu\mp\sqrt{(\gamma+2\mu)^2+4\ell_2}\right)\quad\text{and}\quad\Lambda_{P2}=\frac{1}{2}\left(\gamma-2\mu\mp\sqrt{(\gamma+2\mu)^2-4\ell_2}\right),$$

respectively. The first pseudo equilibrium $\boldsymbol{x}_{P1}$ is unstable as the real part of the second eigenvalue is positive, whereas the second pseudo equilibrium $\boldsymbol{x}_{P2}$ is stable for $\gamma\in(0,\rho\sqrt{1+\mu^2}-\mu(1-\omega^2)$ but unstable for $\gamma>\rho\sqrt{1+\mu^2}-\mu(1-\omega^2)$.

5. Global analysis of synchronous periodically impacting limit cycles

{globalsec}

In this section existence conditions for the simplest type of limit cycles for the full system in which the periodic orbits have one instantaneous impact are derived analytically and are supported by numerical calculations. We show that these invariant sets undergo smooth fold bifurcations and new non-smooth Hopf-like bifurcations, i.e. at the BEB regular and pseudo equilibria as well as two limit cycle bifurcate. In §6 we give a local analysis of the latter in a more general setting. We also discuss the stability of these limit cycles in §5(a) and codimension-2 bifurcations related to the Hopf-type bifurcation (dependence on the stiffness related parameter ω) in §5(b). Having

considered equilibrium solutions we now study the simplest type of limit cycle in our system (3.3). These, period T periodically impacting limit cycles, experience one impact per cycle with identical impact velocity $\dot{U}(t_{i,-})$ at each impact event at time t_i for $i = 0, 1, 2 \ldots$. We further assume that these impacts occur synchronously with respect to the rotating framework. As a consequence the impact position $U(t_i)$ is identical at each impact at time t_i. In summary, we will study the periodically impacting limit cycles which satisfy repeatable initial conditions between consecutive impacts at time t_i and t_{i+1} given by

$$\boldsymbol{w}(t_{i,-}) \equiv \begin{pmatrix} U(t_i) \\ \dot{U}(t_{i,-}) \end{pmatrix} = \begin{pmatrix} U(t_{i+1}) \\ \dot{U}(t_{i+1,-}) \end{pmatrix} \equiv \boldsymbol{w}(t_{i+1,-}) \tag{5.1}$$ {eqRcond}

where we abbreviate the notation to $U_i = U(t_i)$ and $\dot{U}_{i,-} = \dot{U}(t_{i,-})$. It follows that, in polar coordinates, the normal and tangential velocity components must satisfy $\dot{r}_{i,-} = \dot{r}_{i+1,-}$ and $\dot{\theta}_{i,-} = \dot{\theta}_{i+1,-}$. We will show that for certain values of the damping parameter γ a finite number of such limit cycles coexist with a regular equilibrium. We will then demonstrate that only one set of a pair of physically plausible limit cycles with different period T undergoes a discontinuity induced bifurcation (DIB) at the BEB point $\gamma = \gamma^* =: \gamma_{DIB}$. That bifurcation will be shown to be of *non-smooth Hopf* type as two cycles collide with the boundary equilibrium point as their amplitude shrinks to zero. We conclude with illustrations for cases in which these limit cycles are physically realistic and for which they are stable.

A systematic approach to studying the limit cycles of the hybrid system comprising smooth flows between instantaneous impacts, is to consider the map from one impact event to the next. In particular, to determine the existence and stability of such limit cycles of period $T = t_1 - t_0$ it is equivalent to investigate the fixed points of the impact map P_I defined by

$$\begin{aligned} P_I &: \Sigma \to \Sigma \\ \boldsymbol{w}(t_{i,-}) &\mapsto P_I\big(\boldsymbol{w}(t_{i,-})\big) = \boldsymbol{w}(t_{i+1,-}) \end{aligned}$$

Such fixed points ($i = 1$) of period T, $\boldsymbol{w}(t_{0,-})$, satisfy the conditions

$$\boldsymbol{w}(t_{1,-}) = \boldsymbol{w}(t_{0,-}) \quad \text{or equivalently} \quad (t_1, \theta_1, \dot{r}_{1,-}, \dot{\theta}_{1,-}) = (t_0 + T, \theta_0 + 2\pi, \dot{r}_{0,-}, \dot{\theta}_{0,-}).$$

As before $\Sigma \subset \mathbb{R}^n$ denotes the impact surface (4.2). The advantage of this construction is that we can reduce the dimension of the problem by one as the radial coordinate $r = 1$, when the rotor is in contact with the boundary. Note that the set of solutions can include trajectories which are physically implausible in that they exit the interior of the bearing. However, these can be detected numerically once the existence conditions have been obtained.

To find fixed points, $\boldsymbol{w}_{0,-}$, we substitute the repeatable initial condition (5.1) into the general solution of the flow given by (3.3)

$$\boldsymbol{w}_{0,-} = \exp(AT)(\boldsymbol{w}_{0,+} + A^{-1}\boldsymbol{b}) - A^{-1}\boldsymbol{b}$$

where A and $\boldsymbol{b}$ are given in (3.2), and where the real part of the eigenvalues of A, given in (3.4), is negative, i.e. $\mathrm{Re}(\lambda_\pm) = -\gamma/2 < 0$ for $\gamma > 0$. Now, we solve for $\boldsymbol{w}_{0,-}$ to obtain

$$\boldsymbol{w}_{0,-} = -\big(\exp(-AT) - I\big)^{-1} \begin{pmatrix} 0 \\ q\dot{r}_{0,-}U_0 \end{pmatrix} - A^{-1}\boldsymbol{b}. \tag{5.2}$$ {eqFP}

The matrix expression can be simplified further by considering the eigendecomposition of $A = VDV^{-1}$. Then

$$\begin{aligned} \big(\exp(-AT) - I\big)^{-1} &= \frac{1}{1 - \mathrm{tr}\left(\exp(AT)\right) + \det\left(\exp(AT)\right)} \Big(\exp(AT) - \det\left(\exp(AT)\right) I\Big) \\ &= \frac{1}{1 - \mathrm{tr}\left(\exp(DT)\right) + \exp\left(\mathrm{tr}(AT)\right)} \Big(\exp(AT) - \exp\left(\mathrm{tr}(AT)\right) I\Big) \end{aligned}$$

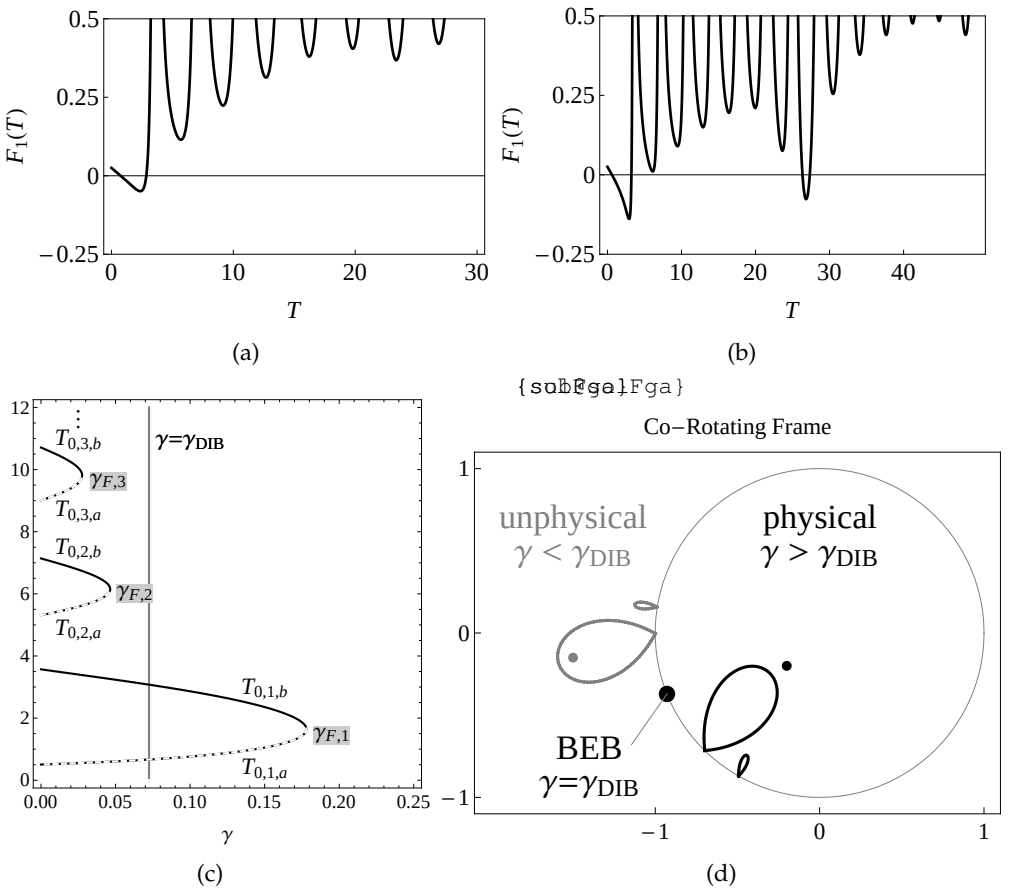

Figure 4: The form of the function $F_1(T)$ for fixed parameters $\omega = 0.76$, $d = 0.95$ and $\mu = 0.15$ with $\gamma = 0.1$ shown in (4a) and with $\gamma = 0.05$ shown in (4b). In (4c) we show the zeros of $F_1(T)$ as the damping coefficient γ is varied ($\omega = 0.76,\ d = 0.95,\ \mu = 0.15,\ \gamma_{F,1} \approx 0.178,\ \gamma_{DIB} \approx 0.072$). In (4d) we show a schematic of the Non-smooth Fold–Hopf-type Bifurcation of the regular equilibrium $\boldsymbol{x}_R$ (dot) and the two limit cycles $B_{1,a}$ and $B_{1,b}$.

by Jacobi's formula. Finally, we can use the eigenvalues of A, λ_+ and λ_-, given in (3.4), to obtain

$$\big(\exp(-AT) - I\big)^{-1} = \kappa \begin{pmatrix} \nu_- e^{\lambda_+ T} - \nu_+ e^{\lambda_- T} - e^{(\lambda_+ + \lambda_-)T} & \nu_+\nu_-(e^{\lambda_- T} - e^{\lambda_+ T}) \\ e^{\lambda_+ T} - e^{\lambda_- T} & \nu_- e^{\lambda_- T} - \nu_+ e^{\lambda_+ T} - e^{(\lambda_+ + \lambda_-)T} \end{pmatrix}$$
$$=: \begin{pmatrix} a_{11}(T) & a_{12}(T) \\ a_{21}(T) & a_{22}(T) \end{pmatrix}$$

where $\nu_\pm = -\lambda_\pm/(1 - \omega^2 - i\gamma)$ and $\kappa = 1/((1 - e^{\lambda_- T})(1 - e^{\lambda_+ T})(\nu_- - \nu_+))$. Hence substituting this matrix into (5.2) simplifies to

$$\boldsymbol{w}_{0,-} \equiv \begin{pmatrix} U_0 \\ \dot{U}_{0,-} \end{pmatrix} \equiv \begin{pmatrix} e^{i\theta_0} \\ (\dot{r}_{0,-} + i\dot{\theta}_{0,-})U_0 \end{pmatrix} = \begin{pmatrix} -q\, a_{12}(T)\, \dot{r}_{0,-} U_0 + k \\ -q\, a_{22}(T)\, \dot{r}_{0,-} U_0 \end{pmatrix} \tag{5.3}$$

where $k = \rho e^{i\phi}/(\omega^2 - 1 + i\gamma)$. The system (5.3) yields three equations by solving the first row equation for U_0, taking the real part of the second row equation and solving it for $\dot{r}_{0,-}$, and

taking the imaginary part of the second row equation, respectively,

$$U_0(1 + a_{12}(T)\, q\, \dot{r}_{0,-}) = k \tag{5.4}$$ {eqFP3a}

$$\dot{r}_{0,-}\left(1 + \mathrm{Re}(q\, a_{22}(T))\right) = 0 \tag{5.5}$$ {eqFP3b}

$$\dot{\theta}_{0,-} = -\,\mathrm{Im}\left(q\, a_{22}(T)\right)\dot{r}_{0,-} \tag{5.6}$$ {eqFP3c}

To determine the fixed points $\boldsymbol{w}_{0,-}$ from (5.3), we first find the period T, unknown a priori, from (5.5) and then compute the corresponding values $\dot{r}_{0,-}$ from (5.4), θ_0 from (5.4) and $\dot{\theta}_{0,-}$ from (5.6). Now, (5.5) is satisfied if $\dot{r}_{0,-}$ is zero, which only yields the boundary equilibrium $\boldsymbol{x}_B$, or if the nonlinear term in T, denote it by $F_1(T)$, is zero. Hence the period T can be determined by finding the zeroes of $F_1(T)$, given by

$$F_1(T) := 1 + \mathrm{Re}\left(q\, a_{22}(T)\right) = 1 - \mathrm{Re}\left(\frac{q}{\lambda_+ - \lambda_-}\left(\frac{\lambda_+ e^{\lambda_+ T}}{e^{\lambda_+ T} - 1} - \frac{\lambda_- e^{\lambda_- T}}{e^{\lambda_- T} - 1}\right)\right) \tag{5.7}$$ {funF1}

$$= 1 + \frac{(1+d)e^{-\gamma T/2}}{s_1}\left(\frac{s_2^- e^{\gamma T/2} - 2s_3^- e^{\gamma T}\cos(s_4^- T + \zeta^-)}{2(1 + e^{\gamma T} - 2e^{\gamma T/2}\cos(s_4^- T))} + \frac{-s_2^+ e^{\gamma T/2} + 2s_3^+ e^{\gamma T}\cos(s_4^+ T + \zeta^+)}{2(1 + e^{\gamma T} - 2e^{\gamma T/2}\cos(s_4^+ T))}\right) \tag{5.8}$$

where $s_1 = \sqrt{4\omega^2 - \gamma^2}$, $s_2^{\mp} = 2 \mp s_1 + \gamma\mu$, $s_3^{\mp} = \sqrt{(1+\mu^2)(1+\omega^2 \mp s_1)}$, $s_4^{\mp} = (\mp 2 + s_1)T/2$, $s_5^{\mp} = \pm\gamma + (\mp 2 + s_1)\mu$, and $\zeta^{\mp} = 2\arctan(s_5^{\mp}/(s_3^{\mp} + s_2^{\mp}))$.

We now consider the analytic form of $F_1(T)$. It is evident from (5.7) that it is oscillatory in T. If $\gamma > 0$ then the oscillations have decreasing amplitude as the period T increases and $F_1(T)$ tends to one as T tends to infinity. If T is fixed and $\gamma > 0$ increases then the amplitude of the oscillations also decreases to zero. Furthermore, if we fix γ and assume that T is large, then

$$F_1(T) \approx 1 + \frac{(1+d)e^{-\gamma T/2}}{s_1}\left(-s_3^- \cos(s_4^- T + \zeta^-) + s_3^+ \cos(s_4^+ T + \zeta^+)\right) \tag{5.9}$$

and is bounded, i.e. $F_1^-(T) < F_1(T) < F_1^+(T)$ where

$$F_1^{\pm}(T) = 1 \pm \frac{(1+d)e^{-\gamma T/2}}{s_1}\left(s_3^- + s_3^+\right). \tag{5.10}$$

The upper and lower bounds $F_1^{\pm}(T)$ are positive for all large T. Therefore, for fixed parameters, and if $\gamma > 0$ the nonlinear function $F_1(T)$ has finitely many zeroes. This is consistent with the plots presented in figures 4a and 4b. As γ is decreased and the amplitude of the oscillations of F_1 increase then more zeroes arise pairwise. Moreover, if γ is zero then $F_1(T)$ is purely oscillatory and hence has infinitely many zeroes.

The period T depends on the damping parameter, γ, the stiffness, ω, the coefficient of restitution, d, and the coefficient of friction, μ. Therefore varying unbalance radius ρ, or unbalance angle ϕ will not affect it. We illustrate the period's dependence on γ in a bifurcation plot for fixed parameters $\omega = 0.76$, $d = 0.95$ and $\mu = 0.15$ (figure 4c). This figure not only illustrates the existence of a finite number of zeroes for $\gamma \in (0, \gamma_{F,1} \approx 0.178)$ and hence of fixed points of the map P_I of a period T but also that no such fixed points exist otherwise.

The next variable, normal impact velocity, $\dot{r}_{0,-}$, can now be determined from T by taking the absolute value of (5.4) and solving for $\dot{r}_{0,-}$. Then for each value of the period T, $\dot{r}_{0,-}$ has two solutions $\dot{r}_{0,-,a}$ and $\dot{r}_{0,-,c}$ given by

$$\dot{r}_{0,-,c/a}(T) = \frac{-g(T) \pm \sqrt{g(T)^2 - |q|^2|a_{12}(T)|^2(1 - |k|^2)}}{|q|^2|a_{12}(T)|^2} \tag{5.11}$$ {eqrd}

where $g(T) = (1+d)\left(\mathrm{Re}\left(a_{12}(T)\right) - \mu\,\mathrm{Im}\left(a_{12}(T)\right)\right)$.

However, we observe that these solutions may themselves coalesce at a fixed bifurcation at $\gamma = \gamma_F^- \approx -0.497$ (figure 5a). But as γ_F^- is negative it has no physical context on the application. As γ is increased these two branches persist under varying stability and admissibility.

A fixed point is potentially *admissible* if the rotor is approaching the impact surface from within the clearance circle, i.e. $\dot{r}_{0,-} > 0$. Otherwise ($\dot{r}_{0,-} < 0$), it is *virtual*. Note that one of the radial velocities (5.11) becomes zero if $1 - |k|^2 = 0$, i.e. when $\gamma = \gamma^*$. In figure 5 it becomes evident that only low normal impact velocity fixed points undergo a sign change in $\dot{r}_{0,-}$.

The angle at impact θ_0 and the tangential impact velocity $\dot{\theta}_{0,-}$, do not need any constraints imposed upon them to ensure admissibility. From (5.4) and (5.6) we obtain their expressions, respectively,

$$\theta_0(T, \dot{r}_{0,-}) = \operatorname{Arg}\left(\frac{k}{1 + a_{12}(T) q \dot{r}_{0,-}}\right) \tag{5.12}$$ {funth}

$$\dot{\theta}_{0,-}(T, \dot{r}_{0,-}) = -\operatorname{Im}\Big(q\, a_{22}(T)\Big)\dot{r}_{0,-} \tag{5.13}$$ {funthd}

which are determined by T and $\dot{r}_{0,-}$. Note that the unbalance phase ϕ has no effect on the fixed points, i.e. it shifts the angle at impact θ_0 but does not change the nature of the dynamics. In fact, ϕ could have been scaled out of the equation. Furthermore, to satisfy the equivalent scaled condition for the relative tangential velocity, (2.2), the tangential velocity $\dot{\theta}_{0,-}$ would have to be greater than -40 taking pre- and post-impact values into account. This is the case as shown in Figure 5c and 5d. We can now summarise the main result concerning the period T periodic points.

{prop2}

Proposition 5.1. *Let $n \in \{1, \ldots, N\}$ and $m \in \{a, b, c, d\}$.*
If there exists a period $T_{0,n,m}$ such that

$$F_1(T_{0,n,m}) = 0$$

then there are finitely many (up to $2N$), period T periodic points $B_{n,m}$ given by

$$B_{n,m} = (T_{0,n,m},\ \theta_{0,n,m},\ \dot{r}_{0,-,n,m},\ \dot{\theta}_{0,-,n,m}) \tag{5.14}$$ {eqprop1}

with $T_{0,n,m}$, $\theta_{0,n,m}$, $\dot{r}_{0,-,n,m}$ and $\theta_{0,-,n,m}$ determined by the equations (5.7), (5.12), (5.11) and (5.13), respectively. Two pairs of fixed points, $B_{n,a}$ and $B_{n,c}$, and $B_{n,b}$ and $B_{n,d}$, have the same period, i.e.

$$T_{0,n,a} \equiv T_{0,n,c} \quad \text{and} \quad T_{0,n,b} \equiv T_{0,n,d}.$$

If $\gamma \in (0, \gamma^*)$ then half of the fixed points, $B_{n,a}$ and $B_{n,b}$, are virtual and the other half, $B_{n,c}$ and $B_{n,d}$, are admissible.

Proof. If the damping coefficient $\gamma > 0$ then, as stated above, $F_1(T)$ has finitely many zeroes $T_{0,n,m}$. Now, let $n \in \{1, \ldots, N\}$ and $m \in \{a, b, c, d\}$. Then for each $T_{0,n,a}$ two normal impact velocities, $\dot{r}_{0,-,n,a}$ and $\dot{r}_{0,-,n,c}$ can be computed from (5.11) and hence $\theta_{0,n,a}$ and $\theta_{0,n,c}$ from (5.12) and $\dot{\theta}_{0,-,n,a}$ and $\dot{\theta}_{0,-,n,c}$ (5.13). Thus we obtain two different periodic points, $B_{n,a}$ and $B_{n,c}$ given by (5.14), with the period $T_{0,n,a}$. For the purpose of nomenclature set $T_{0,n,c} = T_{0,n,a}$. Due to the oscillatory character of $F_1(T)$ its zeros arise pairwise, i.e. there exists a second zero $T_{0,n,b}$. Assume that $T_{0,n,b} \neq T_{0,n,a}$ then the equivalent result follows for $B_{n,b}$ and $B_{n,d}$.

Assume $\gamma \in (0, \gamma^*)$ then $|k|^2 > 1$. Assume further that there exists a period $T_{0,n,a}$. Consider

$$\dot{r}_{0,-,n,a} := \dot{r}_{0,-}(T_{0,n,a}) = \frac{-g - \sqrt{g^2 - |q|^2|a_{12}|^2(1 - |k|^2)}}{|q|^2|a_{12}|^2} < \frac{-g - |g|}{|q|^2|a_{12}|^2} \leqslant 0.$$

Similarly,

$$\dot{r}_{0,-,n,c} := \dot{r}_{0,-}(T_{0,n,a}) = \frac{-g + \sqrt{g^2 - |q|^2|a_{12}|^2(1 - |k|^2)}}{|q|^2|a_{12}|^2} > \frac{-g + |g|}{|q|^2|a_{12}|^2} \geqslant 0.$$

The same holds for the period $T_{0,n,b}$. Therefore the fixed points $B_{n,a}$ and $B_{n,b}$ are virtual but $B_{n,c}$ and $B_{n,d}$ are admissible. □

Proposition 5.2. *Let $n \in \{1, \ldots, N\}$ and assume that the fixed points $B_{n,m}$ exist for all $m \in \{a, b, c, d\}$. Then at $\gamma = \gamma_{F,n}$ for fixed n there are two simultaneous smooth fold bifurcations to which the fixed points coalesce, i.e. $B_{n,a}$ and $B_{n,b}$ meet at the first fold and $B_{n,c}$ and $B_{n,d}$ at the other.*

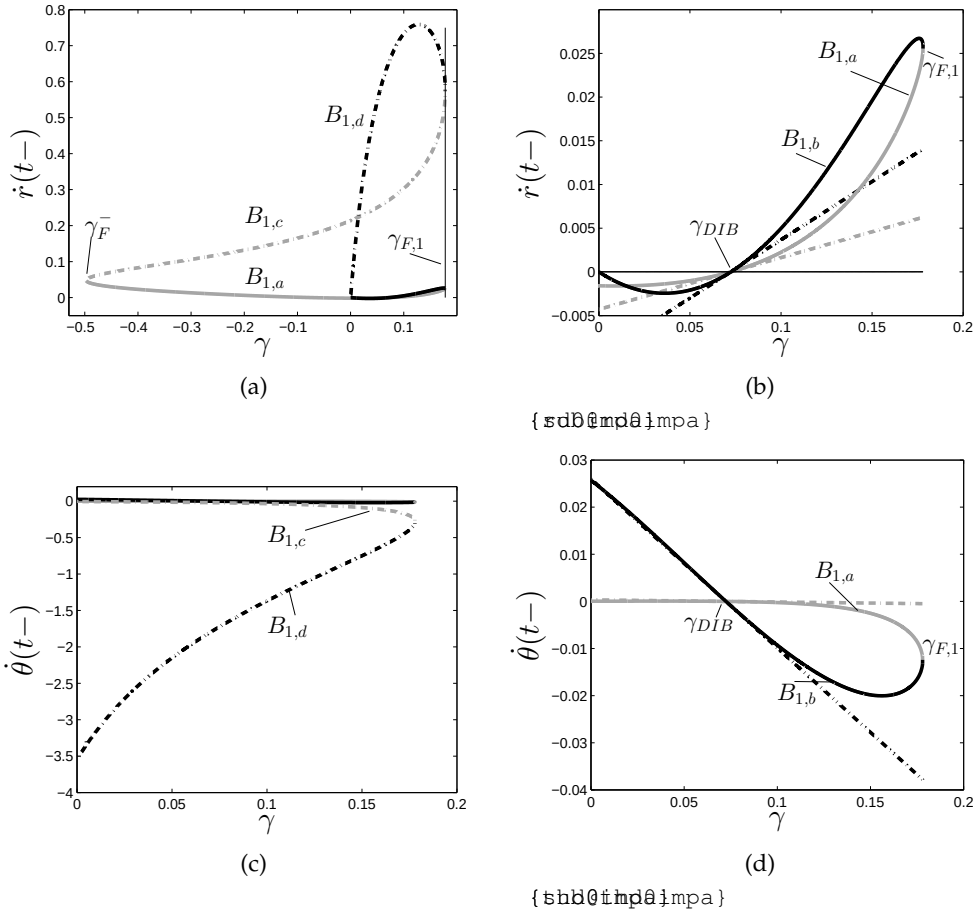

{rd0impa} {rd0impb}

{rd0impa} {rd0impb}

Figure 5: (a) and (b) Normal impact velocity of the four fixed points $B_{1,m}$. (a) The two fixed points $B_{1,a}$ and $B_{1,c}$ coalesce at $\gamma_F^- \approx -0.497$. (b) Enlarged view of (a) of the two fixed points $B_{1,a}$ and $B_{1,b}$ and now including the respective estimate of the fixed points obtained by the local linearisation of the system described in §6. ($\gamma_{DIB} \approx 0.072$). (c) and (d) Tangential impact velocity $\dot{\theta}(t-)$ of the four fixed points $B_{1,m}$ with $m = a, b, c, d$. (d) Enlarged view of (c) of the two fixed points $B_{1,a}$ and $B_{1,b}$ and now including the respective estimate of the fixed points obtained by the local linearisation of the system described in §6.

{rd0imp}

Proof. As stated above, the function F_1 has finitely many zeros for any $\gamma > 0$ and an infinite number as $\gamma \to 0$. Furthermore, F_1 is a smooth function of γ and has regular quadratic minima. It follows, that as γ decreases, then zeros arise pairwise at regular fold bifurcations at points $\gamma_{F,n}$. Let $n \in \{1, \ldots, N\}$ and $m \in \{a, b, c, d\}$. Assume $0 < \gamma < \gamma_{F,n}$ and that the fixed points $B_{n,m}$ exists. Then there exist γ, $T_{0,n,a} \equiv T_{0,n,c}$ and $T_{0,n,b} \equiv T_{0,n,d}$ with $T_{0,n,a} \neq T_{0,n,b}$ such that

$$F_1(T_{0,n,a}, \gamma) = F_1(T_{0,n,b}, \gamma) = 0.$$

as $F_1(T)$ is oscillatory with decreasing amplitude due to $\gamma > 0$. By the continuity of $F_1(T, \gamma)$ there exists $\gamma = \gamma_{F,n}$ such that

$$T_{0,n,a} = T_{0,n,b} =: T_{0,n,F}.$$

Then for each n and $T = T_{0,n,F}$ there exist two fixed points $B_{n,a}$ and $B_{n,c}$. For $\gamma > \gamma_{F,n}$ the nonlinear function $F_1(T)$ has no zeroes. Hence for each n two pairs of fixed points coincide at $\gamma = \gamma_{F,n}$, i.e. $B_{n,a}$ and $B_{n,b}$ bifurcate in a smooth fold bifurcation and so do $B_{n,c}$ and $B_{n,d}$. □

A numerical example of the this bifurcation at $\gamma = \gamma_{F,n}$ is depicted in figures 4c and 5a.

Now let us turn to the question of admissibility. If $0 < \gamma_{F,N} < \gamma^*$ then the low impact velocity branches $B_{n,a}$ and $B_{n,b}$ are virtual for all n whereas the other two, $B_{n,c}$ and $B_{n,d}$ are admissible by proposition 5.1.

However, in the other case, $\gamma_{F,N} > \gamma^*$, further information about $\dot{r}_{0,-,n,m}$ is required. If $\dot{r}_{0,-,n,m}$ is increasing as γ is increasing then all four fixed point sets are admissible. Otherwise they are virtual.

In either case the normal velocity $\dot{r}_{0,-}$ of a pair of fixed points, $m = a, b$ or c, d, changes sign, figure 5b, leading one to anticipate a discontinuity-induced bifurcation, setting the scene for the main result of this paper.

Proposition 5.3. *Let $n \in \{1, \dots, N\}$ and assume that the fixed points $B_{n,m}$ exist $\forall m = a, b, c, d$. Assume further that $\gamma_{F,1} > \gamma^*$, ω satisfies the non-smooth fold condition (4.5) and that $\dot{r}_{0,-,1,m}$ is increasing as the damping parameter γ is increasing.*

Then at the BEB point

$$\gamma = \gamma^* =: \gamma_{DIB}$$

a more general discontinuity-induced bifurcation occurs. The fixed point pairs, $B_{n,a}$ and $B_{n,b}$, clash with the regular nonimpacting equilibrium $\boldsymbol{x}_R$ and the pseudo equilibrium $\boldsymbol{x}_{P1}$. As γ decreases through γ_{DIB} the four invariant sets switch from being admissible to virtual.

We call this a subcritial non-smooth *Fold–Hopf bifurcation* (NSFH).

Proof. Let $\gamma = \gamma^*$. Then either $\dot{r}_{0,-,n,a} = 0$ or $\dot{r}_{0,-,n,c} = 0$ by (5.11). Consequently, by (5.2), it follows that

$$\boldsymbol{w}_{0,-} = -A^{-1}\boldsymbol{b} = \begin{pmatrix} k \\ 0 \end{pmatrix} = \boldsymbol{w}_{0,+}.$$

Therefore the fixed point corresponds to the equilibrium solution $\boldsymbol{w}(t) = -A^{-1}\boldsymbol{b}$, which is the boundary equilibrium $\boldsymbol{x}_B$. Hence as the impact velocity $\dot{r}_{0,-,n,a} = 0$ increases through $\gamma = \gamma^*$ it undergoes a sign change corresponding to the limit cycle transitioning from physically implausible to plausible. Taking proposition 4.1 into consideration it follows that a clash of two limits cycles $B_{n,a}$ and $B_{n,b}$ and two equilibria $\boldsymbol{x}_R$ and $\boldsymbol{x}_{P1}$ occurs. □

A schematic of this phenomenon in r, θ phase space is illustrated in figure 4d. Our statement is further supported by numerical examples such as figure 7a where the limit cycles corresponding to fixed points $B_{1,a}$ and $B_{1,b}$ are depicted. Their amplitudes, $\min(r(t))$ between impacts at times t_i and t_{i+1}, increase as γ decreases and clash with the boundary, the regular equilibrium $\boldsymbol{x}_R$, and pseudo equilibrium $\boldsymbol{x}_{P1}$.

Although we have identified under what conditions pairs of fixed points $B_{n,m}$ are admissible, their physical plausibility is not guaranteed as it is possible that between impacts the corresponding limit cycle trajectory has a further impact.

In order to demonstrate whether such an impact occurs we present the numerical analysis for our model example. We compute the trajectories of the corresponding fixed points $B_{1,m}$ and plot all local extrema of $r(t)$ between impacts $t \in (t_i, t_{i+1})$, figure 7. The branches, $B_{1,a}$, $B_{1,b}$ and $B_{1,c}$ are not affected by this phenomenon unlike the limit cycle corresponding to the fixed point $B_{1,d}$. As γ is decreased a grazing event [29] (orbit lies tangential to Σ with zero normal impact velocity) occurs, i.e. amplitude $r(t)$ crosses the impact surface at $\gamma = \gamma_{\text{graze}} \approx 0.0636$, figure 7b.

Furthermore, these numerical calculations indicate that fixed point pairs with high normal impact velocity, $B_{n,c}$ and $B_{n,d}$ with $n > 1$, are virtual. We believe this to be the case as these pairs only exist for $\gamma \in (0, \gamma_{\text{graze}})$, where the orbit of the corresponding limit cycle exceeds the boundary. In §6 we extend this result using a local linearised system to give more precise results.

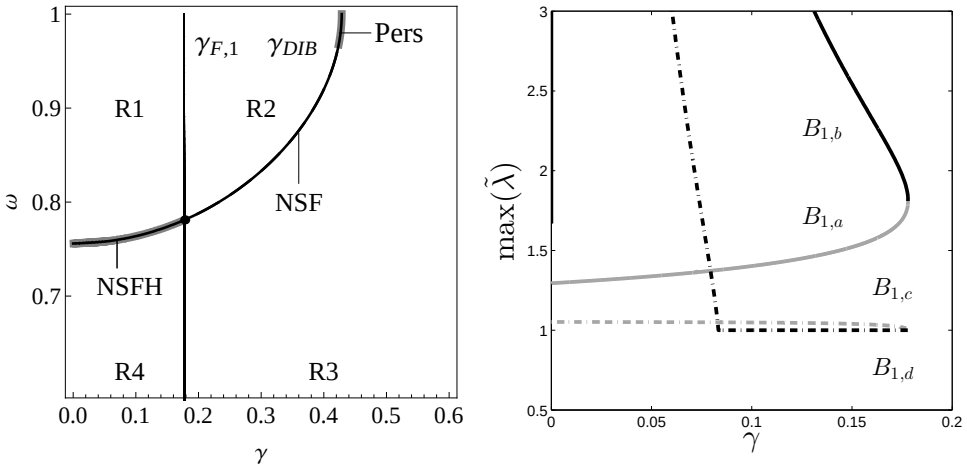

{codim2f} {subfigvalf}

Figure 6: (a) Co-dimension-2 bifurcation by varying damping γ and stiffness ω. (b) Eigenvalue analysis yields only one stable fixed point $B_{1,d}$ for $\gamma > 0.0834$

{co2stab}

(a) Stability analysis

{StabAna}

In the following we present the stability analysis of the fixed points of the impact map P_I. In particular, we focus on the first pair of fixed points, i.e. $B_{1,m}$ with $m = a, b, c, d$, as these appear to be the only physically plausible ones, as shown in the previous section. Their stability is determined by the eigenvalues $\tilde{\lambda}$ of the Jacobian matrix

$$J(B_{1,m}) = \begin{pmatrix} \frac{\partial t_1}{\partial t_0} & \frac{\partial t_1}{\partial \theta_0} & \frac{\partial t_1}{\partial \dot{r}_{0,-}} & \frac{\partial t_1}{\partial \dot{\theta}_{0,-}} \\ \frac{\partial \theta_1}{\partial t_0} & \frac{\partial \theta_1}{\partial \theta_0} & \frac{\partial \theta_1}{\partial \dot{r}_{0,-}} & \frac{\partial \theta_1}{\partial \dot{\theta}_{0,-}} \\ \frac{\partial \dot{r}_{1,-}}{\partial t_0} & \frac{\partial \dot{r}_{1,-}}{\partial \theta_0} & \frac{\partial \dot{r}_{1,-}}{\partial \dot{r}_{0,-}} & \frac{\partial \dot{r}_{1,-}}{\partial \dot{\theta}_{0,-}} \\ \frac{\partial \dot{\theta}_{1,-}}{\partial t_0} & \frac{\partial \dot{\theta}_{1,0}}{\partial \theta_0} & \frac{\partial \dot{\theta}_{1,-}}{\partial \dot{r}_{0,-}} & \frac{\partial \dot{\theta}_{1,-}}{\partial \dot{\theta}_{0,-}} \end{pmatrix}.$$

It is evident that determining this matrix analytically is difficult as the general solution to (3.3) in polar coordinates is a complicated nonlinear function. But we can compute the Jacobian eigenvalues numerically. In figure 6b we present $\max(|\tilde{\lambda}|)$ of the four fixed points illustrating that $B_{1,a}$, $B_{1,b}$ and $B_{1,c}$ are unstable for all γ and that $B_{1,d}$ is quasi-periodically stable for $\gamma \in (0.083, \gamma_{F,1})$ but unstable otherwise. Taking into account the results from the previous section it is evident that as γ decreases from $\gamma_{F,1}$ the fixed point $B_{1,d}$ becomes unstable before it undergoes grazing .

(b) Codimension-2 bifurcation

{codim2bif}

We complete this section with a codimension-2 bifurcation analysis studying the coalescence of various bifurcation points. Of interest is the influence of other parameters on the NSFH bifurcation. Certain magnetic bearing parameters are constrained due to the system's characteristics such as coefficient of friction, μ, or restitution, d, which are governed by material properties. Stiffness, however, can be more easily adjusted through the PID control. Hence we have chosen ω to be the second bifurcation parameter.

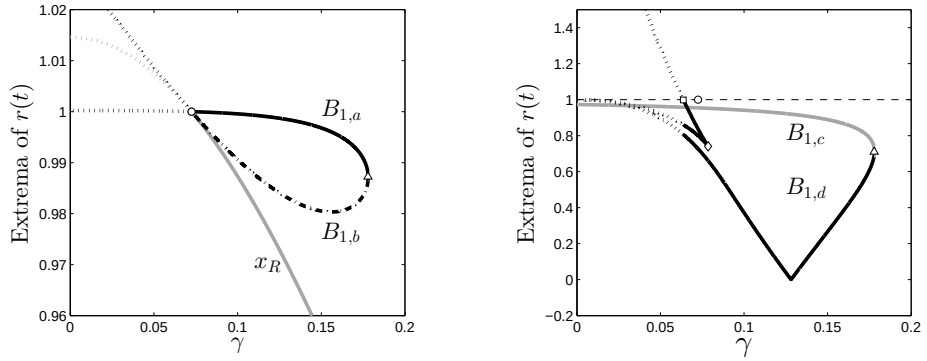

{subfigmaa} {subfigmab}

Figure 7: Bifurcation diagram of γ against local extrema of $r(t)$ for $t \in (t_i,\, t_{i+1})$ for fixed point pairs a) $B_{1,a}$ and $B_{1,b}$ and b) $B_{1,c}$ and $B_{1,d}$. ($\gamma_{F,1} \approx 0.178$ ($\triangle$)). In a) we also plot the regular equilibrium $\boldsymbol{x}_R$ to illustrate the non-smooth Fold–Hopf bifurcation at $\gamma_{DIB} \approx 0.072$ ($\circ$). Figure b) depicts a grazing bifurcation at $\gamma \approx 0.0636$ ($\square$) after an increase in the number of local extrema of $r(t)$ at $\gamma = 0.0785$ ($\Diamond$)

{xtrema}

For our particular example, $\mu = 0.15$, $d = 0.95$ and $\rho = 3/7$, we analyse the smooth fold at $\gamma_{F,1}$ of the first fixed point set $B_{1,m}$ and the DIB point, $\gamma_{DIB} = \sqrt{\rho^2 - (1-\omega^2)^2}$, as we vary γ and ω (figure 6a).This shows that $\gamma_{F,1}$ and γ_{DIB} coincide at $\gamma \approx 0.178$ and $\omega \approx 0.781$, and that four critical regions can be identified (not taking pseudo-equilibria into account):

R1: The three invariant sets $\boldsymbol{x}_R$, $B_{1,a}$ and $B_{1,b}$ are virtual, whereas $B_{1,c}$ and $B_{1,d}$ are admissible.
R2: No fixed points exist and the regular equilibrium $\boldsymbol{x}_R$ is virtual.
R3: No fixed points exist and $\boldsymbol{x}_R$ is admissible.
R4: All invariant sets $B_{1,m}$ and $\boldsymbol{x}_R$ are admissible.

This demonstrates that three types of non-smooth bifurcation between equilibria and/or period T limits cycles occurs, i.e. the already known NSF and persistence (Pers) bifurcations and the new NSFH bifurcation, on the boundary of regions **R1** and **R2**. We observe that the limit cycle corresponding to $B_{1,d}$ undergoes a grazing event in regions **R1** and **R2**. Identifying this grazing set is part of future work.

6. Generalised local analysis of the Hopf-type bifurcation

{localsec}

The global analysis of this specific nonlinear system implies that limit cycles bifurcate in pairs at a non-smooth Fold–Hopf-type bifurcation from a boundary equilibrium point. We now examine this bifurcation in more detail locally by considering a locally linearisation of the system described earlier close to the bifurcation point. This allows us to perform the local analysis for a more general system which includes the one discussed in Section 5. The purpose of this section is two fold. On the one hand we can establish the conditions for the existence of two fixed point solutions of the impact map P_I with period T given by the solutions of the equation (6.4). On the other hand we also obtain a more precise description of the local behaviour of the periodic solutions. We find that the estimates obtained by this analysis agree well with the calculations given in §5. To do this local analysis we consider the complex linear differential equation in $\boldsymbol{w} = (z, \dot{z})$

$$\dot{\boldsymbol{w}} = A\boldsymbol{w} + \boldsymbol{b} \quad \text{in } |z| < \sigma \tag{6.1}$$

{eqgeneral}

with a reset law applying at $|z| = \sigma$

$$\dot{z}_+ - \dot{z}_- = -(1+d)(1+i\mu)\,\mathrm{Re}(z^* \dot{z}_-)\frac{z}{|z|^2} \tag{6.2}$$

where

$$A = \begin{pmatrix} 0 & 1 \\ -\beta & -\alpha \end{pmatrix} \quad \text{and} \quad \boldsymbol{b} = \begin{pmatrix} 0 \\ \Gamma \end{pmatrix}.$$

Our basic assumptions are that there exist parameters α_0, β_0 and Γ_0 such that

$$\left|\frac{\Gamma_0}{\beta_0}\right| = \sigma$$

and that the eigenvalues of the matrix A have negative real part. These conditions imply that at the critical parameters there is a stable boundary equilibrium as is the case for the bearing problem.

We now consider the dynamical behaviour of solutions which are small perturbations to this situation. To do this we introduce a small real parameter ε and consider the perturbed system coefficients (6.1) with

$$\alpha \sim \alpha_0 + \varepsilon\alpha_1,\ \beta \sim \beta_0 + \varepsilon\beta_1 \text{ and } \Gamma \sim \Gamma_0 + \varepsilon\Gamma_1$$

and the same reset law (6.2). From here onwards we use the symbol $\sim$ to denote equality up to the stated order in ε. We pose the asymptotic solution

$$z(t) \sim z_0 + \varepsilon z_1(t), \quad \boldsymbol{w}(t) = \boldsymbol{w}_0 + \varepsilon \boldsymbol{w}_1(t)$$

with

$$z_0 = \frac{\Gamma_0}{\beta_0} = \sigma e^{i\Psi}$$

defining the phase Ψ of z_0 and

$$z_1(t) = r_1(t) e^{i\theta_1(t)}.$$

At order ε

$$\dot{\boldsymbol{w}}_1 \sim A_0 \boldsymbol{w}_1 + \boldsymbol{b}_1 \text{ in } |z| < \sigma$$

where

$$A_0 = \begin{pmatrix} 0 & 1 \\ -\beta_0 & -\alpha_0 \end{pmatrix} \quad \text{and} \quad \boldsymbol{b}_1 = \begin{pmatrix} 0 \\ \Gamma_1 - \beta_1 z0 \end{pmatrix}$$

and $|z| < \sigma$ becomes $|\sigma + \varepsilon r_1(t) e^{i(\theta_1(t) - \Psi)}|$ or

$$\varepsilon r_1(t) \cos(\theta_1(t) - \Psi) < 0.$$

There is an equilibrium at $z_0 = \Gamma_0/\beta_0$, $z_1 = (\Gamma_1 - \beta_1 z_0)/\beta_0$. Defining real constants c and ψ by

$$z_1 = \frac{\Gamma_1\beta_0 - \beta_1\Gamma_0}{\beta_0^2} = c e^{i\psi}$$

the equilibrium lies in $|z| < \sigma$ if

$$\varepsilon c \cos(\psi - \Psi) < 0.$$

In order to find a choice for ε we look at the magnetic bearing example $\beta_0 = \omega^2 - 1 + i\gamma^*$, $\beta_1 = i$, $\Gamma_0 = \rho e^{i\phi}$ and $\Gamma_1 = 0$. Then the expression above becomes

$$-2\varepsilon\gamma^* < 0.$$

As γ^* is positive the equilibrium lies within the clearance circle if ε is negative. By choice of the sign of ε (and hence of Γ_1 and β_0) we may assume that

$$\cos(\psi - \Psi) < 0$$

and hence the stable equilibrium lies inside the clearance circle if $\varepsilon > 0$ but not otherwise. The question we wish to answer is what happens if $\varepsilon > 0$ in this case.

The general solution in $|z| < \sigma$ at order ε is

$$\boldsymbol{w}_1(t) = \exp\Big(A(t-t_0)\Big)(\boldsymbol{w}_{1,0,+} + A_0^{-1}\boldsymbol{b}_1) - A_0^{-1}\boldsymbol{b}_1 \tag{6.3}$$

where $\boldsymbol{w}_{1,0,+} = \boldsymbol{w}_1(t_0+)$ denotes the post impact initial condition. Next we need to find the reset law at order ε and hence consider the impact position first

$$|z(t_0)| = |\sigma e^{i\Psi} + cr_{1,0}e^{i\theta_{1,0}}| = \sigma.$$

This yields a constraint on the angle at impact

$$\varepsilon c r_{1,0}\cos(\theta_{1,0} - \Psi) = 0$$

or $\theta_{1,0} = \Psi + \pi/2$. Deriving the reset law for the impact velocity components requires a few more computations and we shall derive them in stages. Consider the RHS of (6.2)

$$\mathrm{Re}\left(z^*(t_0)\dot{z}(t_{0,-})\right)\frac{z_0}{|z_0|^2} = -\frac{\varepsilon r_{1,0}\dot{\theta}_{1,0,-}}{\sigma}(\sigma e^{i\Psi} + \varepsilon r_{1,0}e^{i\theta_{1,0}}) = -\varepsilon r_{1,0}\dot{\theta}_{1,0,-}e^{i\Psi}$$

where we have substituted for $\theta_{1,0}$. As the LHS of (6.2) can be expressed in the form of

$$\varepsilon\left(i(\dot{r}_{1,0,+} - \dot{r}_{1,0,-}) - r_1(\dot{\theta}_{1,0,+} - \dot{\theta}_{1,0,-})\right)$$

we can now equate the real and imaginary parts of (6.2) to find the reset law at order ε

$$\dot{z}_{1,0,+} = \dot{z}_{1,0,-} + (1+d)(1+i\mu)\, r_{1,0}\, \dot{\theta}_{1,0,-}\, e^{i\theta_{1,0}}$$

As in the problem considered earlier, this system may have a variety of motions, possibly including chattering behaviour. However, for the purposes of our analysis, we seek solutions which comprise a simple periodic orbit with a single impact. Thus we look for a time of impact $t_1 = t_0 + T$ depending on the previous impact time t_0 and the limit cycle period T. As described in previous sections, such limit cycles satisfy repeatability conditions for position and velocity, given by $z(t_0) = z(t_1)$ and $\dot{z}(t_0-) = \dot{z}(t_1-)$ respectively. The equivalent conditions at order ε are

$$z_1(t_0) = z_1(t_1) \quad \text{and} \quad \dot{z}_1(t_0-) = \dot{z}_1(t_1-).$$

Substituting these into the general solution (6.3) we can obtain the impact maps P_I for the perturbed orbit by solving for the initial conditions $\boldsymbol{w}_{1,0,-} = (z_{1,0}, \dot{z}_{1,0,-})$ that yield period T limit cycles,

$$\boldsymbol{w}_{1,0,-} = -A_0^{-1}\boldsymbol{b} - \begin{pmatrix} a_{11}(T) & a_{12}(T) \\ a_{21}(T) & a_{22}(T) \end{pmatrix}\begin{pmatrix} 0 \\ i(1+d)(1+i\mu)\, r_{1,0}\, \dot{\theta}_{1,0,-} \end{pmatrix} e^{i\theta_{1,0}}$$

where

$$\begin{pmatrix} a_{11}(T) & a_{12}(T) \\ a_{21}(T) & a_{22}(T) \end{pmatrix} := \Big(\exp(-A_0 T) - I\Big)^{-1}.$$

By methods similar to those used in §5 we can find the period T by solving the nonlinear equation

$$F_1(T) := 1 - (1+d)\,\mathrm{Re}\Big((1+i\mu)a_{22}(T)\Big) = 0. \tag{6.4}$$

{chris}

A necessary condition for the existence of such periodic orbits is then given by the requirement that the nonlinear problem (6.4) has a solution T. Note, that such a solution will then describe a family of periodic orbits, parametrised by ε close to the bifurcation point. The period T of the limit cycle only depends on the parameters at the BEB, i.e. α_0 and β_0, and the impact parameters

μ and d. Then the other unknowns determined by T are given by

$$r_{1,0} = \frac{c\left(\ell_3\cos(\psi-\Psi)-\ell_4\sin(\psi-\Psi)\right)}{-\ell_4}, \quad \dot\theta_{1,0,-} = \frac{\cos(\psi-\Psi)}{(1+d)\left(\ell_3\cos(\psi-\Psi)-\ell_4\sin(\psi-\Psi)\right)}$$

$$\dot r_{1,0,-} = \frac{c\cos(\psi-\Psi)\,\mathrm{Im}\left((1+i\mu)a_{22}(T)\right)}{\ell_4}.$$

where

$$\ell_3 := \mu\,\mathrm{Re}\left(a_{12}(T)\right)+\mathrm{Im}\left(a_{12}(T)\right) \quad \text{and} \quad \ell_4 := \mathrm{Re}\left(a_{12}(T)\right)-\mu\,\mathrm{Im}\left(a_{12}(T)\right).$$

Hence it follows that the linearised impact map P_I is given by

$$\theta(t_0) := \arg\left(z(t_0)\right) = \Psi + \frac{r_{1,0}}{\sigma}\,\varepsilon, \quad \dot r(t_0-) = -\varepsilon r_{1,0}\,\dot\theta_{1,0,-}, \quad \text{and} \quad \dot\theta(t_0-) = \varepsilon\dot r_{1,0,-}$$

where the period $T = t_1 - t_0$ is a constant and does not depend ϵ. If we let ε tend to zero then $\theta(t_0)$ tends to Ψ and both $\dot r(t_0-)$ and $\dot\theta(t_0-)$ tend to zero, clearly indicating that the limit cycle resulting from this impact map tends to the boundary equilibrium. Depending on the signs of the parameters, the normal impact velocity switches sign and hence demonstrates the transition from admissible to virtual limit cycle or vice versa giving rise to the NSFH bifurcation. This linearisation agrees with the global analysis from the previous section we illustrate, figure 5b. Furthermore, this is evidence that the NSFH bifurcation can be approximated by a linear impact map in general.

7. Conclusions

A discontinuity induced Hopf–type bifurcation has been shown to exist in rotating machines that may experience impact and friction between a rotor and bearing under contact conditions. Using a particular Poincaré map, the impact map, we have shown that at a subcritical non-smooth Fold–Hopf bifurcation two unstable quasi–periodic limit cycles, a stable equilibrium without impact and a stable pseudo–equilibrium, are created and coexist. For a general linear complex system the local analysis revealed that the impact map is linear in the bifurcation parameter indicating that this phenomenon can be expected in higher dimensional impacting systems.

Other typical impact dynamics such as grazing have been observed which have to be studied further to see if they are a route to chaos via a period adding cascade observed in the $1D$ impact oscillators. We also conjecture that other Hopf-type bifurcations leading, for example, to torus doubling as in [23, 38] could be observed in this system.

The rich dynamics studied in this paper also revealed co-existing smooth fold bifurcations which to our knowledge has not been reported in impacting systems.

Finally, the next essential step is to compare this simplified model to experimental data from rigid magnetic bearing systems and determine how much of the qualitative dynamics discussed in this paper remains.

Acknowledgment

K.M. gratefully acknowledges the financial support of the Engineering and Physical Sciences Research Council (EPSRC) Doctoral Training Grant (DTG) and the University of Bath. P.G. was partially funded by EPSRC grant EP/E050441/1 (CICADA). We are grateful to the anonymous referees who's helpful comments have led to an improvement in the paper.

References

1 A.R. Bartha. *Dry friction backward whirl of rotors*. PhD thesis, ETH. Zürich, Switzerland, 2000.

2 J. J. B. Biemond, A. P. S. de Moura, C. Grebogi, N. van de Wouw, and H. Nijmeijer. Dynamical collapse of trajectories. *EPL Europhys. Lett.*, 98(2):20001, 2012.

3 H.F. Black. Interaction of a whirling rotor with a vibrating stator across a clearance annulus. *J. Mech. Eng. Sci.*, 10(1):1–12, 1968.

4 C. Budd and F. Dux. Chattering and related behaviour in impact oscillators. *Phil. Trans. R. Soc. A*, 347(1683):365–389, 1994.

5 D.W. Childs. Rub-induced parametric excitation in rotors. *ASME J. Mech. Des.*, 101:640–644, 1979.

6 D.W. Childs. Fractional–frequency rotor motion due to nonsymmetric clearance effects. *ASME. J. Eng. Power*, 104:533–541, 1982.

7 M.O.T. Cole. On stability of rotordynamic systems with rotor–stator contact interaction. *Proc. R. Soc. A*, 464(2100):3353–3375, 2008.

8 M. di Bernardo, C.J. Budd, A. Champneys, P. Kowalczyk, A. Nordmark, G. Tost, and P. Piiroinen. Bifurcations in nonsmooth dynamical systems. *SIAM Rev.*, 50(4):629–701, 2008.

9 M. di Bernardo, C.J. Budd, A.R. Champneys, and P. Kowalczyk. *Piecewise-smooth dynamical systems: theory and applications*. Springer-Verlag, London, 2008.

10 M. di Bernardo, A. Nordmark, and G. Olivar. Discontinuity-induced bifurcations of equilibria in piecewise-smooth and impacting dynamical systems. *Phys. D*, 237(1):119–136, 2008.

11 F.F. Ehrich. Bistable vibration of rotors in bearing clearance. In *ASME, Winter Annual Meeting, Chicago, ILL*. ASME 65-WA/MD-1, 1965.

12 F.F. Ehrich. High order subharmonic response of high speed rotors in bearing clearance. *ASME J. Vib. Acoust. Stress Reliab. Des.*, 110:9–16, 1988.

13 Z.C. Feng and X.Z. Zhang. Rubbing phenomena in rotor-stator contact. *Chaos, Solitons Fract.*, 14(2):257 – 267, 2002.

14 M.R. Jeffrey. Three discontinuity-induced bifurcations to destroy self-sustained oscillations in a superconducting resonator. *Phys. D*, 2011.

15 D.C. Johnson. Synchronous whirl of a vertical shaft having clearance in one bearing. *J. Mech. Eng. Sci.*, 4(1):85–93, 1962.

16 P.S. Keogh and M.O.T. Cole. Rotor vibration with auxiliary bearing contact in magnetic bearing systems part 1: Synchronous dynamics. *Proc. Inst. Mech. Eng. C J. Mech. Eng. Sci.*, 217(4):377–392, 2003.

17 R.G. Kirk. Evaluation of AMB turbomachinery auxiliary bearings. *ASME J. Vib. Acoust.*, 121(2):156–161, 1999.

18 J.L. Lawen and G.T. Flowers. Synchronous dynamics of a coupled shaft bearing housing system with auxiliary support from a clearance bearing: Analysis and experiment. *ASME J. Eng. Gas Turb. Power*, 119(2):430–435, 1997.

19 R. I. Leine and N. van de Wouw. *Stability and convergence of mechanical systems with unilateral constraints*, volume 36. Springer-Verlag Berlin Heidelberg, 2008.

20 R.I. Leine and D.H. Van Campen. Bifurcation phenomena in non-smooth dynamical systems. *Eur. J. Mech. A-Solid*, 25(4):595–616, 2006.

21 G.X. Li and M.P. Païdoussis. Impact phenomena of rotor-casing dynamical systems. *Nonlinear Dynam.*, 5(1):53–70, 1994.

22 Q.S. Lu, Q.H. Li, and E.H. Twizell. The existence of periodic motions in rub-impact rotor systems. *J. Sound Vib.*, 264(5):1127–1137, 2003.

23 G.W. Luo and J.H. Xie. Hopf bifurcation of a two-degree-of-freedom vibro-impact system. *J. Sound Vib.*, 213(3):391–408, 1998.

24 E.H. Maslen and G. Schweitzer. *Magnetic Bearings: Theory, Design, and Application to Rotating Machinery*. Springer, 2009.

25 K. Mora. *Non-smooth dynamical systems and applications*. PhD thesis, University of Bath, UK, 2013.

26 A. Muszynska. Partial lateral rotor to stator rubs. In *International Conference on Vibrations in Rotating Machinery, 3 rd, Heslington, England*, pages 327–335, 1984.

27 A. Muszynska. Rotor-to-stationary part full annular contact modelling. In *In Proceedings of 9 th International Symposium on Transport Phenomena and Dynamics of Rotating Machinery, Honolulu, Hawaii*, 2002.

28 A. Nordmark, H. Dankowicz, and A. Champneys. Discontinuity-induced bifurcations in systems with impacts and friction: Discontinuities in the impact law. *Int. J. Nonlinear Mech.*, 44(10):1011–1023, 2009.

29 A.B. Nordmark. Non-periodic motion caused by grazing incidence in an impact oscillator. *J. Sound Vib.*, 145(2):279 – 297, 1991.
30 G. Schweitzer. Safety and reliability aspects for active magnetic bearing applications-a survey. *P. I. Mech. Eng. I–J. Sys.*, 219(6):383–392, 2005.
31 D.J.W. Simpson, D.S. Kompala, and J.D. Meiss. Discontinuity induced bifurcations in a model of saccharomyces cerevisiae. *Math. Biosci.*, 218(1):40–49, 2009.
32 D.J.W. Simpson and J.D. Meiss. Andronov–hopf bifurcations in planar, piecewise-smooth, continuous flows. *Phys. Lett. A*, 371(3):213–220, 2007.
33 W.J. Stronge. *Impact mechanics*. Cambridge University Press, 2004.
34 G. Sun, A.B. Palazzolo, A. Provenza, and G. Montague. Detailed ball bearing model for magnetic suspension auxiliary service. *J. Sound Vib.*, 269(3):933–963, 2004.
35 L.P. Tessier. The development of an auxiliary bearing landing system for a flexible AMB–supported hydrogen process compressor rotor. *Proceedings of MAG 97*, pages 120–128, 1997.
36 J.M.T. Thompson and H.B. Stewart. *Nonlinear Dynamics and Chaos*. Wiley, 2002.
37 X. Wang and S. Noah. Nonlinear dynamics of a magnetically supported rotor on safety auxiliary bearings. *ASME J. Vib. Acoust.*, 120(2):596–606, 1998.
38 J. Xie, W. Ding, E.H. Dowell, and L.N. Virgin. Hopf–flip bifurcation of high dimensional maps and application to vibro–impact systems. *Acta Mech. Sin.*, 21(4):402–410, 2005.